Journal Pre-proof

Geochemistry and geochronology of the shallow-level La Esperanza magmatic system (Permian-Triassic), Northern Patagonia

Carmen I. Martínez Dopico, Mónica G. López De Luchi, Augusto E. Rapalini, C. Mark Fanning, Paul Y.J. Antonio

PII: S0895-9811(19)30199-3

DOI: https://doi.org/10.1016/j.jsames.2019.102347

Reference: SAMES 102347

To appear in: *Journal of South American Earth Sciences*

Received Date: 4 May 2019

Revised Date: 2 September 2019

Accepted Date: 2 September 2019

Please cite this article as: Martínez Dopico, C.I., López De Luchi, Mó.G., Rapalini, A.E., Fanning, C.M., Antonio, P.Y.J., Geochemistry and geochronology of the shallow-level La Esperanza magmatic system (Permian-Triassic), Northern Patagonia, *Journal of South American Earth Sciences* (2019), doi: https://doi.org/10.1016/j.jsames.2019.102347.

Geochemistry and geochronology of the shallow-level La Esperanza magmatic system (Permian-Triassic), Northern Patagonia

Carmen I. MARTÍNEZ DOPICO[a*], Mónica G. LÓPEZ DE LUCHI[a], Augusto E. RAPALINI[b], C. Mark FANNING[c], Paul Y. J. ANTONIO[d]

[a] - Instituto de Geocronología y Geología Isotópica (INGEIS). Departamento de Geología. Facultad de Ciencias Exactas y Naturales. Universidad de Buenos Aires- CONICET, Buenos Aires, Argentina.

[b] - Instituto de Ciencias Básicas, Aplicadas y Ambientales de Buenos Aires (IGEBA). Departamento de Geología. Facultad de Ciencias Exactas y Naturales. Universidad de Buenos Aires- CONICET. Buenos Aires, Argentina.

[c] – Research School of Earth Sciences. The Australian National University, Mills Road, Canberra, Australia

[d] - Instituto de Astronomia, Geofísica e Ciências Atmosféricas (IAG), Universidade de São Paulo (USP), São Paulo, SP, Brazil

* Corresponding author Tel: +541159243034. Email: carmen.martinez.dopico@gmail.com;

ABSTRACT

The La Esperanza plutonic-volcanic complex is the largest Late Paleozoic-Early Triassic composite magmatic system of northern Patagonia. This paper reports new SHRIMP U-Pb zircon ages and K-Ar muscovite dating as well as whole-rock geochemical data for selected units. In addition, we present some new and reprocessed whole-rock Sr isotopic compositions. On the basis of the new and published data, three compositionally and isotopically distinct high-K magnesian calc-alkaline series were distinguished. Two of these are characterized by high Ba-Sr: (i) biotite and muscovite bearing rhyolites and granites (265 ± 2 Ma; 260 ± 2 Ma) and (ii) metaluminous amphibole-biotite bearing granodiorites (273 ± 2 Ma), monzogranites (255 ± 2 Ma), dacites (253 ± 2 Ma), and slightly peraluminous granites (dated herein as 251 ± 2 Ma). There is also a low Ba-Sr series of high-silica metaluminous rocks (granites and acid dike swarms; 250 ± 2 Ma and ≈244 ± 2 Ma). Geochemistry coupled with geochronology revealed a pulsatory multi-sourced open magmatic system with mafic magma replenishment and reactivation of crystal mushes that occurred before upward migration to upper crustal levels. Mafic magmas alternated with crust-derived magmas incrementally assembled in subvolcanic levels over 30 Ma. Zircon crystallization and mica cooling ages in the granite units allowed detection of two magmatic lulls, between 270 and 265 Ma and between 260 and 255 Ma. Both episodes coincide with a period of exhumation in upper crustal levels. The new temporal and geochemical constraints allow correlation of the La Esperanza plutonic-volcanic complex with the Los Menucos Group (258-248 Ma), encompassing a volume of magmatism comparable to a moderately sized large igneous silicic province. These mid-to-late Permian to Middle Triassic rocks record the transition between subduction-related magmatism (>273 Ma) and post-orogenic extensional magmatism (<250 Ma) in the Gondwana margin. Even though this magmatism would be coeval with the proposed collision of the Patagonia terrane, no expected syn-collisional magmatism or associated deformation were found in upper crustal levels. However, the different nature and melting conditions of the inferred sources of the magmas that crystallized before 270 Ma, between

265 and 260 Ma, and from 255 to 245 Ma, suggest that the La Esperanza plutonic-volcanic complex was assembled during a 30 Ma period of major plate reorganization.

Keywords: Patagonia; La Esperanza; Permian- Triassic SLIP; Giménez Granite; U-Pb zircon geochronology

INTRODUCTION

The igneous rocks in the La Esperanza area have received much attention since Ramos (1984) proposed the allochthonous origin of Patagonia. Their isolated location far away from already suspected Paleozoic active margins, the calc-alkaline character of the rocks and alleged Carboniferous ages (subsequently corrected to Permo-Triassic; Pankhurst et al., 1993) together with the deformation in Late Paleozoic rocks of Sierra de la Ventana, were the three strongest arguments that the rocks in La Esperanza were an active magmatic arc with pre- to syn-collisional stages. Pankhurst et al. (2006) proposed that this magmatism was the result of a thermal anomaly in the upper plate (i.e. post-collisional magmatism) postdating the earlier Carboniferous collision of the Deseado Massif and the North Patagonian Massif (Fig.1a). Recently, Luppo et al. (2019) found anomalous paleomagnetic pole positions for the 265-252 Ma volcanic rocks around La Esperanza, whereas the paleomagnetic poles of rhyolite dikes dated at 244±2 Ma were consistent with the pole position for Middle-Triassic in most reference paths for South America.

The aim of this paper is to present the magmatic stratigraphy, geochronological and geochemical backgrounds of a very well exposed example of a shallow composite magmatic system, the La Esperanza plutonic-volcanic complex of northern Patagonia (Llambías and Rapela, 1984; Martínez Dopico et al., 2013, 2017a), to provide a framework to test future hypotheses regarding the potential cogenetic evolution of the magmas. We report new SHRIMP U-Pb zircon data and two K-Ar muscovite dating as well as WR geochemical data for selected units. In addition, we present some new and reprocessed whole-rock Sr isotopic compositions and review Hf and O (in zircon) and whole rock Nd-isotope data published for the area.

GEOLOGICAL BACKGROUND

The La Esperanza plutonic-volcanic complex crops out in the surroundings of La Esperanza settlement (“Estancia La Esperanza Nueva”, 19G 543350 E 5525800 UTM coordinates), in central Río Negro province, Patagonia, Argentina. The Estancia La Esperanza is located 170 km to the south of

Neuquén and 60 km to the north of Los Menucos (Fig.1a). Permian to Triassic igneous rocks are distributed in an area of over 1000 km^2 (conservatively), although recent regional correlations (Luppo et al., 2018, 2019) suggest that the magmatic event could have extended over more than 3000 km^2 beneath large areas covered by the Cenozoic Somun Curá volcanic plateau.

The geology of the La Esperanza area was described in detail by Llambías and Rapela (1984) who proposed the terms "La Esperanza plutonic complex" and "Dos Lomas volcanic complex" to distinguish the plutonic suites from the volcanic and volcaniclastic rocks, subvolcanic leucogranites and dikes. These complexes were thought to be separated by a regional unconformity. This former stratigraphy, followed by Cucchi et al. (2001), was modified by Martínez Dopico et al. (2013b) with the hypothesis of a single magmatic plumbing system built by the assembly of magma batches and termed it the La Esperanza plutonic-volcanic complex. Rapela and Llambías (1985) and Martínez Dopico et al. (2013, 2014) studied the geochemistry of the pre-Jurassic units, describing a meta- to slightly peraluminous, magnesian, high-K calc-alkaline granite series that evolved through a combination of processes such as mixing and fractional crystallization of magmas from at least two different sources (Martínez Dopico, 2013).

The first reliable time constraints for these rocks were established with WR Rb-Sr isochrons yielding late Permian to Middle Triassic ages (Pankhurst et al 1993), superseding previous mistaken Carboniferous ages. U-Pb zircon crystallization ages were provided by Pankhurst et al. (2006), and after by Martínez Dopico et al. (2017b) and Luppo et al. (2019). Together with thermochronological data (Martínez Dopico et al. 2013, 2017b), mica cooling ages bracketed the evolution of the rocks between mid-Permian (Kungurian-Roardian) and Middle Triassic (Anisian). Sm-Nd, Lu-Hf and O isotopic data are available from Pankhurst et al. (2006), Fanning et al. (2011) and Castillo et al. (2017).

LA ESPERANZA PLUTONIC-VOLCANIC COMPLEX

The exposures of igneous rocks around Estancia La Esperanza cover an area larger than 2500 km^2, where mid-Permian to Middle Triassic intrusions and associated volcanic products were mapped as La Esperanza plutonic-volcanic complex (LEPVC) (Fig. 1b). The intrusive rocks of the LEPVC crop out as small scattered and flat bodies, whereas the volcanic and subvolcanic counterparts constitute a dome (known as a *rhyolite dome* in Llambías and Rapela, 1984), and a large mostly eroded plain (Fig. 1b). These rocks are intruded by several generations of large super-acidic dike swarms and leucogranite plugs that stand out above the regional topography as ridges. Volcanic rocks are distributed along a N-S elevated axis that extends 45 km to the south, from the puesto Llanquil to the Piche Graben (outside our area of interest). Spatial distribution is affected by E-W transform faults (Giacosa et al., 2005). The regional host rocks of the LEPVC are the Early Paleozoic phyllites and quartzitic schists of the Colo Niyeu Formation (Labudía and Bjerg, 1994; Martínez Dopico et al., 2017c), which are intruded by the oldest unit of the complex, the Prieto Granodiorite, 30 km to the SW of Estancia La Esperanza.

The geochemical data provided in this paper is a compilation of the whole-rock major and minor elements of Rapela and Llambías (1985), major, minor and trace elements of Martínez Dopico (2013), mineral chemistry of Martínez Dopico et al. (2013a) and new data representative of the main units of the LEPVC.

Intrusive units

Geochemical and field data allow recognition of four main mappable units among the subvolcanic intrusions: 1) Prieto Granodiorite; 2) Donosa Granite and muscovite-bearing aplite dikes; 3) La Esperanza Monzogranite; and 4) Giménez Granite (Fig. 1b).

Prieto Granodiorite

This unit crops out to the north and south of the Estancia La Esperanza and its surrounding areas (Fig. 1b) and partially corresponds to Prieto Granodiorite of Llambías and Rapela (1984). The granodiorite dated at 273 ± 2 Ma by Pankhurst et al. (2006) belongs to this unit. The granodiorite bodies were emplaced as large horizontal layers in the border of the complex or as N-S aligned vertical feeders (magma conduits, see Martínez Dopico et al., 2017a). The Prieto Granodiorite is in fault contact with the Donosa Granite and is covered by younger volcanic and subvolcanic rocks to the east of Estancia La Esperanza. Biotite-amphibole granites, granodiorites and minor diorites (modal classification) displaying a wide range of textures and compositions make up the Prieto Granodiorite (63-70% SiO_2; $3<K_2O<4\%$; MgO>2%; 0.84<ASI<0.93; $La/Yb_N \approx 13$). The rocks are dominantly dark grey, ferromagnetic (10^{-2} SI) and exhibit medium-grained equigranular textures with variable modal contents of mafic minerals (Fig. 2a). They are characterized by euhedral zoned plagioclase (cores An_{45-55} to rims $An_{20-25;}$ see details in Table 6 Supplementary data) (30-35% modal) together with magnesian hornblende (8-15%) and biotite (10%) clots, each of similar size, embedded in K-feldspar (20-30%) and anhedral quartz (20-25%) pools. Pyroxene was occasionally observed as cores of amphibole, particularly in coarse-grained microgranular mafic enclaves. Apatite, zircon, magnetite and titanite are accessory minerals.

La Esperanza Monzogranite

This is a composite pluton that covers half of the studied area. Based on its texture, type of magmatic enclaves, magnetic susceptibility and age, the monzogranites and granites are distinguished from the original "Prieto Granodiorite" of Llambías and Rapela (1984). Two granitoid facies with transitional contacts were recognised; the most extended facies is inequigranular, whereas the other encompasses porphyritic granites and crops out exclusively around puesto Calvo. The inequigranular facies crops out in the easternmost sector of La Esperanza as a subhorizontal layer or sill, whereas in the west, the spatial distribution of its outcrops reflects the NNW-SSE and NW-SE anisotropies of the basement (Martínez Dopico et al., 2017a). This facies comprises grey, variably ferromagnetic (10^{-3}-10^{-2} SI), inequigranular granodiorites and monzogranites (63-68% SiO_2; $3<K_2O<4\%$; MgO<2%; 0.90<ASI<1.13; $20<La/Yb_N<30$) in which euhedral plagioclase (or K-feldspar) is embedded in a matrix of granitic composition. It is characterized by euhedral zoned plagioclase (cores An35–45 to rims An20-25; Table 6 Supplementary data, 30-45% modal), euhedral biotite and Mg-hornblende clots (color index<18%), poikilitic filiform perthitic K-feldspar (20-30%) and anhedral quartz (20-30%). Allanite, zircon and titanite are accessory minerals. In the Arroyo del Corral (Fig. 1b), the inequigranular monzogranites of La Esperanza are observed intruding the Donosa Granite. Close to puesto Calvo, K-feldspar megacrysts are developed, amphibole disappears and the color index drops to <5% (porphyritic granite; 68-71% SiO_2; $3<K_2O<4\%$; MgO<1.2%; 0.9<ASI<1.0; $K \approx 10^{-3}$ SI), and porphyritic microgranular mafic enclaves are also present (Fig. 2b). In the field, these granitoids are isotropic. However, in several localities north of puesto Donosa and to the east of puesto Linconao very fine-grained rocks exhibit macroscopic magmatic foliation due to a weak shape-preferred orientation of ferrosilicates or plagioclase crystals: in such rocks, the color index rises to 25%. Rounded mafic microgranular enclaves are very abundant and display two types: (i) up to 15 cm long rounded and very dark, porphyritic (plagioclase) enclaves (Fig. 2b) and (ii) small fine-grained equigranular enclaves. The mineralogical composition of the enclaves is identical to that the host. The inequigranular monzogranite facies was dated as 255 ± 2 Ma using U-Pb SHRIMP methodology on magmatic zircons (Martínez Dopico et al., 2017a). This age agrees with K-Ar mica cooling ages and stratigraphic relations (Fig.1b); see Martínez Dopico et al., (2017b) for further discussion.

Donosa Granite

This unit is the core of the complex. It crystallized at 260 ± 2 Ma (Martínez Dopico et al., 2017a) and comprises a pink euhedral K-feldspar megacrystic granite. Its discontinuous outcrops describe a large N-S elongated body with NW-SE and SW-NE, fault-related, rectilinear borders. Several E-W and SW-NE dextral faults dismember the pluton and there are isolated outcrops along the E-W and NE-SW valleys to the west of Estancia La Esperanza. The Donosa Granite is in fault contact with the Prieto Granodiorite in its northern and western margins and it is covered by the Collinao Dacite to the east. Donosa granites exhibit oversized pink euhedral K-feldspar megacrysts up to 15 x 4 cm. Field measurements indicate a dominant NNW-SSE orientation of megacrysts with a slight NW plunge. Excluding this magmatic lineation, the main N-S body is mostly isotropic. However, along the Arroyo del Corral valley, locally ductile magmatic shear bands and porphyritic synmagmatic dikes are common. These bands are defined by the alignment of biotite and pseudotachylite material that crosscut the rock and create areas of orthogneiss. Some K-feldspar megacrysts display a domino alignment when associated with shear band sense of movement. These deformational features were usually detected close to the contact with the more dioritic components of the Prieto Granodiorite. Other evidence of brittle and ductile deformation such as autobrecciation and development of decimetric zones of orthogneiss were found. Fine-grained pink muscovite-bearing leucogranite dikes are associated with this unit (e.g. sample DZ35a; Table 3).

The most outstanding feature of the Donosa granites ($K \approx 10^{-3} - 10^{-4}$ SI; 71-76% SiO_2; $3.4<K_2O<4.3\%$; MgO<1%; 0.95<ASI<1.10) is the presence of oversized K-feldspar megacrysts. They occur as euhedral perthitic microcline locally showing macroscopic Carlsbad twinning, sodium-rich rims and poikilitic inclusions of quartz. The matrix is monzogranitic and displays equigranular coarse-to-medium grained texture that consists of quartz (20-30% modal), plagioclase (30-40%), perthitic microcline (25-35%) and biotite (<10% modal). Apatite, zircon, monazite, magnetite and muscovite (along borders and cleavage traces of biotite) are accessory minerals. Plagioclase crystals are mostly subhedral, complexly twinned, and show zoning from core (An_{30-20}) to rim (An_{20-15}) (Table 6 Supplementary material). Quartz crystals are subhedral to anhedral, normally forming interstitial clusters and sometimes develop parallel subgrains and chessboard patterns. Biotite is subhedral and greenish-brown, locally intergrown with magnetite. Magnetite is mostly euhedral and free of alteration, although in some sampling sites hematite replacement is widespread. Tourmaline traces were found where decimetric magmatic shear zones develop. Except for local deformation along the E-W Arroyo del Corral, the overall magmatic texture remains unmodified. The transition to the dominant undeformed rock is sharp. In outcrop scale subrounded granite biotite-rich clots occasionally appear. Well- rounded microgranular granodiorite enclaves are rare.

Giménez Granite

This unit crops out to the north of the puesto Giménez area and shows transitional contacts with the inequigranular monzogranites of the La Esperanza Monzogranite. It is typically a fine-grained equigranular pink to pinkish grey granite (70-76% SiO_2; $3<K_2O<5\%$; MgO<1%; 0.90<ASI<1.15) (Fig. 2c). A geochemical transition between these two units was proposed by Rapela and Llambías (1985). Rocks are slightly ferromagnetic ($K\approx10^{-3} – 10^{-4}$ SI). Close to the puesto Giménez, the granite contains K-feldspar (30-40%), plagioclase (25-35%) and quartz (25-30%) with variable amounts of biotite (5-15%). Magnetite, apatite, zircon and scarce monazite are accessory minerals. K-feldspar is euhedral, characteristically zoned and perthitic. Plagioclase crystals are subhedral and zoned, with core composition ranging from An_{42} to An_{38} and strongly sodic rims ($<An_{10}$), sometimes myrmekitic. Quartz is anhedral and exhibits low-to-medium temperature deformation features such as chessboard extinction, subgrain development and bulging structures. Biotite is subhedral, brown-yellow colored. In the field, these granites are mostly isotropic, although NW-SE (130-150º) trending magmatic foliation with variable dip was observed in a few localities.

Further north of the puesto Giménez, around Ruta Nacional 67, the granite develops a porphyritic texture with K-feldspar megacrysts up to 12 cm-long embedded in a granite matrix (megacrystic granite facies; Fig. 2d). The matrix is composed of K-feldspar, plagioclase, quartz, biotite, minor quantities of muscovite and accessories such as zircons, magnetite and apatite. The K-feldspar megacrysts are euhedral and locally exhibit shadow tails. They are inhomogenously distributed but locally concentrated with their major axes defining steep lineations. K-feldspar megacrysts are thought to concentrate through mechanical accumulation during constricted magma flow in pipes (Paterson et al., 2005). Flattened equigranular biotite rich-schlieren and plagioclase aggregates up to 10 cm are abundant. The schlieren consist mostly of biotite and andalusite (plus cordierite) surrounded (replaced) by muscovite (chlorite). Andalusite might be considered as a restitic or peritectic phase whereas individual crystals of euhedral biotite apparently crystallized from the melt. Foliated metamorphic enclaves are also observed. Further northeast, these rocks are transitionally interfingered with a grey banded porphyritic muscovite-biotite granodiorite in synmagmatic folds. The attitude of these banded rocks is NNW-SSE, dipping to the west. The megacrystic granites are sharply interlayered and intruded by a grey biotite-bearing tonalite (herein named Álvarez Tonalite; 66-70% SiO_2; $2<K_2O<3\%$; MgO<2%; 1.03<ASI<1.12) in which magmatic foliation is depicted by the alignment of plagioclase crystals.

Extrusive units

Among (semi)extrusive rocks formerly known as the Dos Lomas plutonic-volcanic complex (Llambías and Rapela, 1984), seven units have been distinguished: 1) Pailemán Rhyolite composed of rhyolite, ignimbritic rhyolite and vitrophyre, 2) Pailemán breccias, and 3) Llanquil Fm. making up the rhyolite dome; 4) andesite dikes; 5) Collinao Dacite made up of (a) ignimbritic dacite and rhyodacite, and (b) dacite; 6) Calvo Granite; and 7) Acidic dikes of (a) aplite and leucogranite and (b) porphyritic rhyolite (Fig. 1b).

Pailemán Rhyolite and related lithologies

The Pailemán Rhyolite crops out in the central to northern parts of a dome-shaped body (the “rhyolite dome” of Llambías and Rapela, 1984) ca. 8 km northeast of Estancia La Esperanza. The unit corresponds to the mid and upper sections of high-viscosity rhyolitic lava plugs and black and purple vitrophyres (Fig. 3a). The Pailemán rhyolites are porphyritic with a high proportion of phenocrysts to matrix. They consist of subhedral to anhedral quartz, subhedral and partially broken crystals of zoned plagioclase, variable amounts of K-feldspar, muscovite, ferromagnesian minerals (biotite) and opaque minerals set in a devitrified groundmass. Feldspar phenocrysts are perthitic and partially replaced by sericite and clay minerals whereas ferromagnesian minerals are replaced by chlorite aggregates. A representative rock of the rhyolite dome, a muscovite-bearing rhyolite was dated with U-Pb SHRIMP zircon data at 264 ± 2 Ma (Pankhurst et al., 2006).

The **Llanquil Formation** is an epiclastic volcanic microbreccia (Fig. 3b) associated with the volcanic dome that comprises a series of very small outcrops in the western slope of the southernmost part of a SSE-NNW valley that dissects the Pailemán dome. It is crosscut by felsic microgranite dikes.

In the eastern part of the rhyolite dome, an autoclastic rhyodacitic breccia (herein called Pailemán Breccia) overlies the Prieto Granodiorite. It is a porphyroclastic rock with a high proportion of phenoclasts to matrix (>60%) which shows several episodes of brecciation. Phenoclasts show great variation in size, reaching up to a centimetre; the phenoclastic fraction is composed of mainly subhedral rounded and partially broken quartz and subhedral non-zoned plagioclase, biotite (their proportions are widely variable) and very minor amount of opaque minerals. Alteration is pervasive and mainly affects plagioclase and biotite. Secondary muscovite was seen. The groundmass is inhomogeneous showing different degrees of crystallinity with perlitic, felsitic and microgranular textures. There are amphibole bearing-xenoliths with pilotaxic groundmass textures.

Collinao Dacite

This comprises a mainly greenish-grey porphyritic dacite with occasional eutaxitic textures (62-69% SiO_2; K_2O<4%; 5<$MgO+Fe_2O_{3t}$<8%; 0.8<ASI<1.1) (Fig. 3c). The original name of the unit given by Llambías and Rapela (1984) was Collinao dacitic ignimbrite. However, examination in more than 15 localities only revealed one with ignimbritic texture, so we consider it more accurately referred to as a lava rather than an ignimbrite. The phenocryst mineral assemblage is dominated by plagioclase (up 50 vol. % in the coarser grained types), amphibole, biotite, Fe–Ti oxides, quartz and apatite (trace). The groundmass varies from fine-grained micropoikilitic crystalline with the development of snowflake textures and interstitial quartz to felsitic–microgranular in the subvolcanic types. Groundmass minerals are feldspar and quartz with small grains of amphibole, biotite and opaque minerals, titanite and apatite microlites. Amphibole is the dominant ferromagnesian mineral in the quartz-poor dacites. Close to the puesto Collinao (Fig. 1b), the groundmass comprises plagioclase microlites set in the poikilitic groundmass and the only ferromagnesian phase is biotite. Apatite is abundant and appears either as stubby prisms when associated with amphibole or as acicular crystals in the groundmass. The unit is dated at 253 ± 2 Ma (U-Pb SHRIMP in zircon; Luppo et al., 2019). In the southernmost outcrops of the Collinao Dacite, a subvolcanic facies is exposed comprising a light grey equigranular felsic rock (74-77% SiO_2; K_2O<5%; 5<$MgO+Fe_2O_{3t}$<2%), in which tourmaline aggregates are present. Biotite microgranite dikes with localized coarse-grained pods with quartz-tourmaline miaroles are observed intruding the Collinao Dacite.

Andesitic dikes

All the pre-253 Ma magmatic units are crosscut by <1 m thick, porphyritic to aphyric, dark grey mafic dikes (49-55% SiO_2; K_2O<2%; $Fe_2O_{3t}+MgO$<15%) which, in turn, are crosscut by acid microgranite dikes (Luppo et al., 2019). Mafic dikes with a preferred NE-SW trend (Fig.1b) intrude the Prieto Granodiorite, Donosa Granite and the base of the rhyolite dome. Most are aphyric and composed of euhedral plagioclase in a widely altered fine-grained hornblende and biotite bearing matrix. Other mafic dikes show E-W trends, such as those that intrude the La Esperanza monzogranites and exhibit up to 1 cm euhedral hornblende crystals embedded in pilotaxic to intersertal matrix (lamprophyres).

Calvo Granite and acidic dike swarms.

The Calvo Granite is a silica-rich granite (U-Pb SHRIMP zircon age of 250±2 Ma, Pankhurst et al., 2006) associated with aplite and concentric and radial leucogranitic dikes that constitute the last plutonic activity exposed in the area (246 ± 2 Ma; 244 ± 2 Ma U-Pb SHRIMP zircon ages in Pankhurst et al., 2006; Luppo et al., 2019). The granite crops out as rounded plugs in the surroundings of La Esperanza. It is a medium to coarse grained equigranular pink leucogranite (75-80% SiO_2; 4<K_2O<5%; $MgO+Fe_2O_{3t}$<3%; ASI<1.1) (Fig.3d). In the southern N-S trending outcrop, the granite contains occasional K-feldspar megacrysts and/or the amount of biotite increases, sometimes resembling the

Donosa granites. It contains quartz, K-feldspar and plagioclase, minor amounts of biotite and magnetite (<5%). Garnet has been described to the northeast of Estancia La Esperanza but was not seen by us.

Fine- to very fine-grained granite and banded and/or porphyritic rhyolite dikes intrude all the previous units of this complex (either plutonic or volcanic). In the easternmost sector they are mostly E-W, but in the surrounding of puesto Calvo they radiate following a NE-SW and E-W trend (Fig. 1b). In most cases their length is more than 5 km long and their width between 1-2 m, but porphyritic rhyolite dikes are thicker than the rest and normally form fold hinges in the field. (Fig. 1b). The crosscutting relations between dikes of different orientations are not clear since they change trend imitating a ring structure around the subvolcanic Calvo Granite and thus seem to be related to its emplacement.

GEOCHRONOLOGY

We selected three samples to complete the geochronological framework already published in Pankhurst et al. (2006), Martínez Dopico et al. (2017b) and Luppo et al. (2019) (Table 1).

U-Pb SHRIMP zircon dating

A sample of porphyritic biotite granite 10 km west of Estancia La Esperanza (megacrystic facies of the Giménez Granite) (Z9; 19G 534600 m. E 5525900 m. S) was collected for U-Pb dating on zircons (Fig. 1). Once extracted, zircons were mounted in epoxy together with chips of the Temora standard zircon (Black et al., 2003). Cathodoluminescence (CL) images were used to reveal the internal structures of the polished grains (Fig. 4a). Most zircons were euhedral to subhedral, predominantly translucent and exhibited magmatic zonation (Fig. 4a). Analyses were performed in the SHRIMP RG (Sensitive High-Resolution Ion Microprobe) at the Research School of Earth Sciences of the Australian National University in Canberra according to the protocol outlined in Williams (1998). Data were reduced, statistically analysed and plotted with Isoplot 4.1 (Ludwig, 2003).

Common Pb corrections were made using ^{207}Pb (Williams, 1998). Most zircons were largely euhedral to subhedral, predominantly translucent and exhibit magmatic zonation (Fig. 4a). Twenty-two zircons (27 pits in total) were studied in detail, concentrating on rims but testing potential inheritance in some core–rim pairs (grains #2, 14, 17, 18 and 20; Table 2). We only found Middle Devonian inheritance in only one core of zircon grains. The rest of the cores have shown to have ages between 250 and *ca.* 260 Ma, produced during the same magmatic event. One result (for #14.1) was discarded due to high $f^{206}Pb$ (>5%). The other zircons frequently exhibited parallel zoning and all had Th/U ratios >0.1 and were attributed to a magmatic origin as proposed by Maas et al. (1992). In the Tera-Wasserburg diagram, a tight coherent group on Concordia indicates the crystallization age of this facies of the pluton: 21 $^{238}U/^{206}Pb$ ages gave a weighted mean of 251± 2 Ma (95% confidence level) with a MSWD of 1.4 (Fig. 4b, c). Six zircons ages were ignored because they were either isolated younger (*i.e.,* grain #6 242 Ma) or somewhat older ages (*i.e.,* grains #3, 20 ≈260 Ma), or they had high common lead (*i.e.,* grain #14).

K-Ar white mica dating

Two samples were selected for K-Ar mineral dating from fresh and well exposed areas of acidic and basic dikes from the La Esperanza area. These were Z67b, a coarse-grained variety of the Donosa Granite in Estancia La Esperanza (5443311m E 55527092 mS) and D35a, a medium-grained muscovite-bearing leucogranite dike intruding Prieto Granodiorite 4 km southeast of Puesto Llanquil (554280m E 5531743m S) (Table3).

The samples were crushed in a steel jaw crusher and sieved to isolate the 300–400 µm size fractions. After magnetic separation, muscovite grains from each sample were handpicked under a binocular microscope to obtain homogeneous microcrystalline separates. The purity of the mineral separates is >99%. Clean micas were ground in pure alcohol to remove the possible altered rims that might have suffered a loss of potassium or argon. The K-Ar methodology used is described in Solé

(2009). For potassium analysis X-ray fluorescence with high-dilution fused pearls was used to minimize the matrix effects (Solé and Enrique, 2001). For argon determination a CO_2 laser system was used for sample fusion, followed by gas purification (Solé, 2009). Measurements were performed in a MM1200B noble gas mass spectrometer (Instituto de Geologia, UNAM). Age errors are reported at the 2–σ level (Table 3).

Both samples yielded muscovite-cooling ages of 260±6 Ma, showing rapid cooling of the Donosa Granite, which has a U-Pb zircon crystallization age of 260±2 Ma (Martínez Dopico et al., 2017b).

GEOCHEMISTRY

We present the first complete comparative WR chemical analysis of major, minor and trace elements for the Prieto Granodiorite, La Esperanza Monzogranite, Donosa Granite, Collinao Dacite, Paileman Rhyolite, Calvo Granite, and two acidic dikes from the area of La Esperanza (Table 4). The chemical analyses were conducted at ActLabs, Ontario, Canada under their WRA + trace 4Lithoresearch program. Determinations were performed on samples of up to 5 kg that were screened for alteration in hand specimen and thin sections. Samples were broken using an iron hammer and reduced using an iron-plated jaw crusher and agate mills. X-ray fluorescence spectrometry (XRF) was used for major elements and ICP-MS for trace elements. The precision is better than 1% for major elements and better than 5% for trace elements. The collection was complemented with previous major and some minor elementary data of Rapela and Llambías (1985).

Information was processed using GCDKit 5.0 (Janoušek et al., 2006) and the scripts of Janoušek et al. (2016). In the following text, compositions are expressed recalculated to 100% anhydrous to minimize the effect of alteration on the samples. However, because samples show scatter in alkali contents, we tested the potential effect of secondary processes using the chemical weathering index of Ohta and Arai (2007) (not shown). The great majority of samples follow the predicted igneous trend, except those of the Las Pampas rhyolite and some of the rhyolite dome of Rapela and Llambías (1985), which follow the linear trends for weathering of rhyolites.

Four unpublished Sr isotopic determinations were taken from the data repository of the Instituto de Geocronología y Geología Isotópica (INGEIS): analytical procedures for these were described in Caminos et al. (1988). Initial $^{87}Sr/^{86}Sr$ ratios from the INGEIS data repository, Cingolani et al. (1991) and Pankhurst et al. (1992, 2006) have been recalculated at their respective zircon U-Pb crystallization age and using the ^{87}Rb decay constant of Rotenberg et al. (2012) (Table 5). Whole-rock Nd data from Pankhurst et al. (2006) and zircon-Hf isotopic parameters from Fanning et al. (2011) and Castillo et al. (2017) were recalculated using Sm–Nd CHUR of $^{147}Sm/^{144}Nd = 0.1960 \pm 4$ and $^{143}Nd/^{144}Nd = 0.512630 \pm 11$, and for Lu–Hf CHUR of $^{176}Lu/^{177}Hf = 0.0336 \pm 1$ and $^{176}Hf/^{177}Hf = 0.282785 \pm 11$ of Bouvier et al. (2008).

Geochemical variations

Using the TAS diagram of Middlemost (1994), the Prieto Granodiorite and most of the rocks of the La Esperanza Monzogranite are classified as granodiorites whereas rocks of the base of Collinao Dacite plot as dacites, and andesites. The remaining intrusions and volcanic rocks are compositionally granites or rhyolites.

In the SiO_2-K_2O diagram of Peccerillo and Taylor (1976), most units follow a wide high K- calc-alkaline trend (Fig. 5a) and overlap with that of the partial melts derived from tonalites (Roberts and Clemens, 1993). Basic dikes show a transitional character to the medium-K calc-alkaline series (Fig. 5a). In the granite classification of Frost et al. (2001) all the samples belong to the magnesian series. In the modified alkali-lime index diagram (Fig. 5b) the majority of the rocks (Prieto, La Esperanza, Giménez, Donosa and Collinao units) span the calc-alkalic spectrum with most of them between calc-alkalic and calcic fields. On the other hand, the granites of Calvo intrusion and some acidic dikes are alkali-calcic to calc-alkalic. According to Frost et al. (2001), plutons that are genetically related should plot within the same series. In figure 5b rocks of Calvo Granite seem to be independent from the rest because at the same SiO_2 values, there is a difference in the alkaline-lime ratio. In both bivariate plots is clear that the trends of Prieto Granodiorite, La Esperanza Monzogranite and Collinao Dacite are not subparallel to the proposed lines of chemical differentiation through fractional crystallization within a series (Roberts and Clemens, 1993). Therefore, a significant open-system process such as magma mixing or multiple magma sources may be invoked to explain the variability in the composition of the units. The rocks are mostly metaluminous to slightly peraluminous (ASI ≈1.1) and show variable degrees of alumina saturation within the same unit (Fig. 5c). Minor elements important for granites are Ba, Sr and Rb since they replace Ca and K in feldspars. Comparing the Ba-Sr-Rb compositions of the units (Fig. 5d), two groups can be traced: a group characterized by Ba/Sr>>1, Rb/Ba≥1 and Ce/Sr>1 consisting of the Calvo Granite and the fine-grained acidic dikes ("Low Ba-Sr granites"), and another with Rb/Ba<1, Ba/Sr≥1 Sr/Rb>1 and Ce/Sr<1 or high Ba-Sr granites (Tarney and Jones, 1994). The high Ba-Sr rocks can be further divided by their CaO/K_2O ratio: the Prieto Granodiorite, La Esperanza Monzogranite, Giménez Granite, Collinao Dacite and porphyritic rhyolite dikes have $CaO/K_2O>0.5$, in contrast with the Donosa Granite and Pailemán Rhyolite.

Harker diagrams show that TiO_2, Al_2O_3, CaO, MgO, FeO_t, and P_2O_5 describe inverse relationships relative to SiO_2 for the plutonic-volcanic suite, whereas K_2O and Na_2O increase or show no correlation with SiO_2 (Fig. 6). Al_2O_3 shows a decoupled behaviour of the high and low Sr-Ba groups with a sudden change in the negative slope, a change replicated in the rest of major element trends, particularly in Na_2O and K_2O the trending slope is inverted between the high and low Sr-Ba groups. The different trends seen with alkali-lime index (Fig. 5b) and the sudden change in the slope of the SiO_2-major elements trends (Fig. 6) suggests that the low and high Ba-Sr groups are not related to each other by fractional crystallization and might have been sourced from different protoliths. The variation of Sr versus SiO_2 (Fig. 7) shows a clockwise-trend that also illustrates the behaviour of Ba, Zr, La and Cerium. It is clear from these bivariate diagrams that there are two different segments within each trajectory and a large scatter in the values. In the Prieto

Granodiorite, the La Esperanza Monzogranite and the Collinao Dacite they have a crude positive correlation with SiO_2, while the granites of Donosa and Calvo and the rhyolite dikes show a vertical scatter. Rb and K/Ba plots vs SiO_2 portray anti-clockwise pattern compared to Sr. The variation of Ba, K, Rb within the low-Ba-Sr series (Calvo Granite and fine-grained acidic dikes) suggests K-feldspar fractionation. It is clear from Figure 7 that there is large scatter of Sr and Ba contents in Donosa granites (385-680; 400-1500 ppm, respectively) within a very restricted range of SiO_2 values (73.4-76.0 % weight). The variance of these elements is also large within Giménez granites (265-580; 840-1850 ppm) but within a larger silica range, and with negative correlation between the variables that is not seen in the Donosa Granite. In granites, alkaline earth elements like Sr and Ba are usually mostly contained in feldspars replacing Ca in plagioclase and K in K-feldspar. In both cases, there are rough positive correlations between Sr and atomic Ca but not between Ba and atomic K, suggesting fractionation of Ca-plagioclase. In both cases the span of values in trace elements is rather large to be explained solely by this process. According to Clemens et al. (2010) and Villaros et al. (2009) some alkaline-earth elements, such as Sr, in S-type granites are decoupled from the related major elements because their concentrations in the melts are controlled by local variations in the trace-element contents of the source rocks. Moreover, Sr content and its isotopic composition in the different batches of melt would also depend whether equilibrium melting occurs (see Bea et al., 1996; Farina et al., 2014, among others). As pointed out by Clemens et al. (2009), melts that escape rapidly from the source have less chance to attain equilibrium and may result in lower trace element concentrations compared to those that remain in contact with the source for a long time.

Rare earth element (REE) contents decrease from La to Lu decrease with SiO_2, yielding very low values for the Calvo and Donosa granites and the fine-grained rhyolite dikes (<150 ppm). All units are enriched in light rare earth elements (LREE) and display negatively sloping chondrite-normalized REE patterns (Boynton, 1984) (Fig. 8). The La Esperanza Monzogranite, Collinao Dacite and porphyritic rhyolite dikes (Z19) show very similar patterns with La/Yb_N = 12.2–17.2 and weak negative Eu anomalies (Eu/Eu*=0.70–0.76), whereas the older Donosa Granite and the rhyolite dome have more fractionated patterns with La/Yb_N =20.7-27.7 and weak Eu depletion (Eu/Eu*=0.69–0.76). In contrast, the low Ba-Sr rocks (the Calvo Granite and acid dikes) show 'wing-shaped' chondrite-normalized REE patterns with large Eu negative anomalies (Eu/Eu*=0.36–0.39).

On multi-element diagrams normalised to primitive-mantle-concentrations, the main rocks of the suite exhibit high contents of LILE such as Cs, Rb, Ba, Pb, Th, U and LREE but negative Nb, Ta and Ti, P anomalies. Coupled with the overall high-K character, this suggests a strong crustal characteristic of the magmas, with some mafic to intermediate compositions that should have been derived from lower crustal sources (see below isotopic compositions). The low Ba-Sr acidic granites and rhyolite dikes (75-80 SiO_2 wt%) have a markedly different pattern with larger negative anomalies in Ba, Sr, P, and positive anomalies in HREE (Dy, Y, Yb, Lu). Compared to the upper Continental Crust (Taylor and Mc Lennan, 1995), the low Sr-Ba granites and dikes exhibit dramatically lower contents of Ba, Sr, P and Ti in comparison with the high Ba-Sr rocks. Another thing to note in Fig 8 is that Donosa granites and the rhyolites of the dome have low values of HREE in comparison to the low Ba-Sr rocks at similar SiO_2 contents (i.e. 75% wt). This also suggests that the high and low Sr-Rb rocks cannot be derived from a single parental magma.

Isotope compositions

The 'High Ba-Sr' suite shows a narrow range of mean initial $^{87}Sr/^{86}Sr$ values from 0.7065 (Prieto Granodiorite) and 0.7071 (La Esperanza Monzogranite) to 0.7076 (Donosa Granite). The initial $^{87}Sr/^{86}Sr$ ratios of the volcanic rocks of the rhyolite dome and Collinao Dacite are slightly higher than the plutonic rocks, ranging from 0.7070 to 0.7084, possibly indicating a more crustal (or hybridized) component than the Prieto Granodiorite (Table 5). Similarly, εNdt values for Calvo Granite and volcanic rocks are largely more negative (-7.5<εNdt< -5.8) than those of Prieto Granodiorite (-4.8). Zircon εHft values for the `High Ba-Sr` rocks (-2.9 to -4.6; Prieto Granodiorite) are lower than those of Calvo Granite (-5.6 to -9.0) or rhyolite dikes (-7.4 to -8.7). The initial $^{87}Sr/^{86}Sr$ ratios of the Calvo Granite at 250 Ma are variable (0.6921 to 0.7064) ranging to impossibly low values that could indicate post-crystallization open system behaviour. Only initial $^{87}Sr/^{86}Sr$ ratio of one sample LE132 seems more realistic with values of 0.7064.

Figure 9 shows the initial $^{87}Sr/^{86}Sr$ ratio plotted against SiO_2 for the studied rocks. The main rocks of the high Ba-Sr series, the La Esperanza Monzogranite and Giménez Granite, define a horizontal array, suggesting differentiation from a single parent magma, or at least a common source. The initial $^{87}Sr/^{86}Sr$ ratios of the Donosa Granite are also coincident with this array, but the age difference between the granites of Giménez (*ca.* 250 Ma) and Donosa (260 Ma) precludes a comagmatic relationship, although again a similar source would be possible. Another observation is that the span of initial $^{87}Sr/^{86}Sr$ ratios of the rhyolite dome is similar to that of Donosa Granite (at identical wt % SiO_2) but unrelated to that of the low Sr-Ba series (considering initial $^{87}Sr/^{86}Sr$ values of *ca.* 0.7064). Epsilon Ndt values of Donosa Granite are very negative (-9.8), indicating that the crustal component would be more important than that of the Prieto Granodiorite and the rhyolite dome. However, given the wide spread of εHft zircon values of the rhyolite dome (-3.8 to -8.7), more data is necessary to extract a conclusion out of this unit.

DISCUSSION

Temporal and spatial evolution of the magmatic system

The oldest unit of the area, the Prieto Granodiorite, crystallized at 273 ± 2 Ma (mid Permian, Cissuralian/Guadalupian) according to a U-Pb SHRIMP zircon dating (Pankhurst et al., 2006) for a sample located less than 1 km north of the fault contact with the Donosa Granite (Fig. 4, 10). The crystallization age of the La Esperanza Monzogranite (formerly part of Prieto Granodiorite) is 255 ± 2 Ma (late Permian, Wuchiapingian/Changhsingian), with biotite cooling ages of 248 ± 4 Ma and 251 ± 6 Ma (to the east and west of study area) which reinforce this age (Martínez Dopico et al., 2017b). Initial Sr and Hf isotope ratios and geochemical features suggest a lower crustal source for both units, consistent with their compositional and textural similarities (Martínez Dopico et al., 2017a).

However, the degree of hybridization of the La Esperanza Monzogranite is less than that of the Prieto Granodiorite: it exhibits abundant evidence for mingling whereas the latter is much more homogeneous suggesting less viscosity contrast (i.e. similar temperatures) between interacting melts. On the other hand, emplacement depth differences between them were negligible according to Al-in-hornblende pressure estimates of <2 Kbar (Martínez Dopico et al., 2013a). The Prieto Granodiorite is exposed as the host of the rhyolite dome whose basal unit (i.e. crystaloclastic rhyolite) was dated at 264 ± 2 Ma. However, the rhyolite dome is a complex subvolcanic/volcanic edifice whose age range has not yet been accurately constrained and could extend to Lower Triassic times. Crystallization and cooling of the Donosa Granite in the central part of the main body have been dated as 260 ± 2 Ma (late Permian, Wuchiapingian/Capitanian, U-Pb on zircon age) with a very fast cooling from 400 to 350°C to at 259 ± 6 Ma (K-Ar on muscovite age presented here, Table 3, Fig. 10). Textural evidence of near-surface cooling is seen in the 1-2 cm euhedral crystals of quartz in localities around Arroyo del Corral (Fig.1b), which indicate very fast cooling of the unit and its very shallow character. Muscovite-bearing microgranite dikes (Table 3; sample D35b) could be associated either with the Pailemán Rhyolite or with the Donosa Granite (both rocks contain primary muscovite), and they intrude the Prieto Granodiorite.

Slightly after intrusion of the La Esperanza Monzogranite, the Collinao Dacite was extruded at 253 ± 2 Ma (Luppo et al., 2019) along a N-S trending ridge. The Collinao Dacite clearly overlies the main body of Donosa granites, but contact with the La Esperanza Monzogranite occurs where the granite is highly fractured and altered (Fig.1b). The following event is the intrusion of Calvo Granite, dated at 250 ± 2 Ma by Pankhurst et al. (2006). Although there are no available geochronological constraints on the mafic NW-SE dyke swarm, these dikes intrude the La Esperanza Monzogranite and the Giménez Granite. Therefore, these dikes are constrained as close in time to the extrusion of Collinao Dacite, after the intrusion of Giménez Granite at 251 ± 2 Ma (Figure 1b), but before the ≈244 Ma acid dikes (Luppo et al., 2019). The ≈244 Ma acidic dikes clearly crosscut all the units of the

LEPVC, following E-W, NE-SW and NW-SE trends and are geochemically related to the Calvo Granite (250 ± 2 Ma, Pankhurst et al., 2006).

The unconformity between the La Esperanza plutonic and volcanic rocks

In the first approach to the geology of the La Esperanza magmatic system, Llambías and Rapela (1984) and Rapela and Llambías (1985) divided the rocks around Estancia La Esperanza in two cycles, the first entirely plutonic and the second volcanic and subvolcanic including the Calvo Granite and acidic dikes. Llambías and Rapela (1984) claim "The second Cycle begins after a short erosive period that uncovers the plutonic rocks of the first Cycle and on which in almost horizontal surfaces the first ignimbritic eruptions of dacitic composition (Collinao) were deposited." In the light of the new stratigraphic arrangement (Fig. 10), this simple subdivision does not hold anymore. There is an erosion surface between the Donosa Granite and the Collinao Dacite which is easily seen around Estancia La Esperanza. A second erosion surface might occur between the Permian rocks and the Calvo Granite and associated dikes (<250 Ma). In any case, in the La Esperanza area none of these erosion surfaces seem to represent more than minor adjustments associated with the evolution of the caldera rather than substantial discordances. Further south, rhyolitic ignimbrites, dacite lavas and rhyolitic tuffs at the base and middle sections of the coeval Los Menucos Group (252-258 Ma) were tilted (30º to the east) and intruded by a felsic rhyolite dike swarm equivalent to the group of acidic dikes in La Esperanza. The acidic dikes of the La Esperanza area (Fig. 1) were dated as old as 244 ± 2 Ma (crystallization age of a fine-grained rhyolite dike; Luppo et al., 2019), suggesting that regional uplift and erosion occurred between the emplacement of Calvo Granite (250 ± 2 Ma crystallization age of the northern plug of the Calvo Granite; Pankhurst et al., 2006) and the diking.

Petrogenesis and magmatic kinships

The early Permian Prieto Granodiorite (273 ± 2 Ma) shares major and trace element geochemical characteristics with the late Permian monzogranites and granites of the La Esperanza Monzogranite (255 ± 2 Ma) and its extrusive counterpart, the Collinao Dacite (253±2 Ma). All these rocks contain early crystallizing phases such as orthopyroxene, magnesian clinoamphibole and plagioclase, followed by late hornblende and biotite, titanite and allanite, but lack peraluminous minerals, suggesting that their parental magmas were hydrated and metaluminous. According to the amphibole chemistry of the granodiorites and monzogranites (data in Martínez Dopico et al., 2013) and following the equations of Ridolfi et al. (2010) and Ridolfi and Renzulli (2012), crystallization occurred in similar oxidizing (fO_2 ≈NNO) and hydrous conditions (4>H_2O>5% wt). Minimum crystallization temperatures estimated using the zircon saturation thermometer (TZr, Watson and Harrison, 1983) yielded temperatures of *ca*. 760 ºC for Prieto and La Esperanza granodiorites and *ca*. 800ºC for the later porphyritic granite facies of La Esperanza Monzogranite and Collinao dacites, indicating that magma temperature increased with time. The lack of inherited zircon ages (see Martínez Dopico et al., 2017a; Luppo et al., 2019 and Table 2) and the absence of correlation between Zr and SiO_2 suggest that these are minimum temperatures for the magmas.

Initial $^{87}Sr/^{86}Sr$ ratios, mineralogy as well as crystallization ages suggest that the Giménez Granite is an evolved magma batch (>70% SiO_2) derived from the fractionation of La Esperanza Monzogranite magmas. Major element trends show that it was formed after extensive amphibole and Ca-plagioclase fractionation. All rocks with <70% SiO_2 show coherent Sm/Yb ratios from 3.0 to 4.5, indicating that pyroxene and mainly amphibole were present in the source. This would suggest that the first batch of melt had left hornblende and pyroxene as major residual phases at high T and low P melting conditions of a mafic metaigneous source. Whole-rock initial $^{87}Sr/^{86}Sr$ (0.7064-0.7067; Table 5), Nd (εNd=-4.8)-and zircon Hf isotope compositions (εHf of -2.9 to -4.6; Castillo et al., 2017) for the intermediate rocks of the Prieto Granodiorite are compatible with the interpretation that these magmas were extracted from a mafic or intermediate source with long-term crustal residence. Even though there is a 20 Ma gap between the pulses, the La Esperanza Monzogranite and Giménez

Granite seem to share a common ancestry with the Prieto Granodiorite at the same crustal level. However, the higher initial $^{87}Sr/^{86}Sr$ of the more evolved members of the La Esperanza Monzogranite (porphyritic facies; 0.7070-0.7072) and Giménez Granite (0.7072-0.7075; Table 5) suggest that the felsic component increased with time. The higher abundance of mafic microgranular enclaves in the monzogranites and granites of La Esperanza in comparison with the older rocks indicates that magma hybridization was inefficient. Low zircon $\delta^{18}O$ values for the whole series of rocks of La Esperanza (4.4‰–7.3‰; Castillo et al., 2017) confirm an I-type origin (Valley, 2003). Trace element-based granite tectonic discrimination diagrams (Pearce et al., 1984, 1996; Harris et al., 1986) also point to I-type volcanic arc sources (syn to post-collisional fields) (not shown; see Martínez Dopico et al., 2014).

Granodiorite/dacite, monzogranite and granite of the La Esperanza area yield a wide range of major and trace element concentrations, suggesting variable degrees of partial melting and probably a rapid escape of the magma that prevented further chemical equilibration with the source. The rough negative correlation between SiO_2 and FeO_t, MgO, MnO and TiO_2, and La/Yb_N, Sr, Ba, K, Y and Zr indicates that the fractionation of amphibole and plagioclase might have operated for the crystallization of the Prieto Granodiorite, La Esperanza Monzogranite and Collinao Dacite intermediate magmas, as well as the Giménez Granite. In turn, biotite does not seem to have had an important role since Rb and Ba (both compatible elements in biotite but not in amphibole) do not decrease with SiO_2 or K_2O (Fig.7). The decrease in the Ba content within Donosa would be related to the grain size of the K-feldspar crystals, and, perhaps, related to K-feldspar fractionation. Minor phases that might have controlled the REE fractionation are allanite or monazite. In turn, the middle-Permian Donosa Granite, Ms-bearing leucogranites and the rhyolites of the dome are high-SiO_2 I-type magmas that contain plagioclase as an early crystallizing phase. The growth of muscovite, acid plagioclase and subhedral quartz as well as a disharmonic growth of K-feldspar megacrysts occurred during low-nucleation high-growth rate episode at high-temperature conditions. Hf data in zircons of the rhyolite dome aged between 260-269 Ma show a large variability (-4<εHf-<11; Castillo et al., 2017; Table 5), suggesting either a mixing of sources (mid crustal vs lower crustal) or isotopic disequilibrium melting. Three arguments would preclude a potential derivation of the felsic magmas of the granites of Donosa and rhyolites of the dome from the same source as the Prieto Granodiorite. First, the large REE decoupling between the felsic Donosa Granite (average 73 wt% SiO_2) and the rocks of the rhyolite dome (74 wt% SiO_2) and the intermediate rocks of the La Esperanza Monzogranite and Giménez Granite (72-75 wt% SiO_2). Second, the different whole-rock trace element compositions (high *vs* low Ba-Sr) with similar initial Sr ratios (Table 5). And third, the Nd isotope difference between Prieto Granodiorite (εNd = -4.8) and Donosa Granite (εNd = -9.8). Thus, the Prieto Granodiorite and the La Esperanza Monzogranite could have a mixed crustal - mafic source whereas the Donosa Granite and the Pailemán Rhyolite have a stronger crustal signature. On the other hand, there is no overlap in Sr, Nd and scant overlap in Hf isotopic composition between the <250Ma units, the Calvo Granite and rhyolite dikes, and any other group of rocks. The non-disturbed initial $^{87}Sr/^{86}Sr$ ratios for the early Triassic rocks (<250 Ma) are low (0.7052-0.7064 at 75% SiO_2), coupled with mantle-like O^{18} values (4.4-6.6‰) for zircon with -5.6<εHf <-9.0 units giving the rocks a distinctive signature compared to the older rocks.

Inferences for the tectonic setting and connections with other plutonic or plutonic-volcanic complexes in Patagonia and surroundings

Pankhurst et al. (2006) proposed that the genesis of these calc-alkaline high-K rocks was related to a crustal thickening in the upper plate that following ca 320-305 Ma continental collision of the Deseado Massif and the North Patagonian Massif. The high-K character should not be interpreted as indicating a particular tectonic environment, but rather as a product of the mineralogical and elementary content of mafic sources combined with different degrees of hybridization with felsic materials (e.g., mixing and mingling processes). A primary interpretation of the chemical and isotopic features of these rocks would be that the suitable protoliths for I-type granitic magmas could be related to a previous nearby subduction. Although the volume of mafic rocks within the age range of La Esperanza plutonic-volcanic complex related to the high-K rocks is not significant (e.g., mafic microgranular enclaves and basic dikes), mafic underplating could be invoked as a source of the heat responsible for the magma generation. An alternative process allowing heat in the lower crust is the juxtaposition of the asthenospheric mantle against the base of the crust (i.e. detachment of a subducting slab) and does not require a continental collision. An element that we should start looking at when further isotopic data becomes available is the Hf-isotopic compositions of the inherited zircons aged between 300 and 280 Ma. The εHf values of two zircon rims (inherited) aged 302 and 290 Ma (grains 3.2 and 11.2 of Fanning et al., 2011) of the Calvo Granite (low crystallization TZr ≈ 725 Ma) are -3.7 and -3.8 (recalculated after Fanning et al., 2011) whereas those of igneous zircon in the Prieto Granodiorite vary between -2.9 to -4.6 units. This suggests that zircons aged between 300 and 270 Ma are showing magmas with more positive Hf signatures than those of the latest Permian. At this age, *c.* 300 Ma, massive diorite bodies were dated in the proto-Andean open margin of Gondwana at the same latitude of Estancia La Esperanza, such as the Rahue diorite (WR-mineral Rb-Sr composite isochrons 296±2 Ma, 300±3 Ma; Lucassen et al., 2004) and, further west, the Coastal Batholith (Dekart et al., 2014). Whole-rock initial $^{143}Nd/^{144}Nd$ and zircon initial $^{177}Hf/^{178}Hf$ ratios also point towards a common origin for the Prieto Granodiorite and other older-than-260 Ma plutonic complexes such as Quintuleu Granodiorite in the Mamil Choique complex (281 ± 2 Ma; $-3.6<\varepsilon Hf_t<-4.2$, recalculated after Fanning et al., 2011) in the southwest of the North Patagonian Massif and the granodiorites of the Navarrete plutonic complex (282 ± 2 Ma, Pankhurst et al. (2006); $-3.5<\varepsilon Hf_t<2.9$, recalculated after Fanning et al. (2011); see discussion in Martínez Dopico et al. (2011, 2017a) and Castillo et al. (2017)) (Fig. 10). In turn, for the magmatism after 260 Ma in La Esperanza area, represented by Donosa Granite, La Esperanza Monzogranite and Calvo Granite, isotope data show that the felsic component is higher in the magmatic precursors than those previously molten. The volume of this second stage is larger than the first and corresponds to a major tectonic change with respect to the older conditions. Recent dating and stratigraphic studies (Luppo et al., 2018, 2019) suggest that the plutonic-volcanic event in

La Esperanza area is synchronous and geochemically comparable with the dacites, rhyolites and rhyolitic and dacitic ignimbrites represented by the northernmost expression of the Los Menucos Group (258-252 Ma) (Fig. 10). We propose that La Esperanza-Los Menucos magmatic system meets the criteria proposed by Bryan et al. (2002) to consider it as a "Silicic Large Igneous Province" (SLIP): 1) its bulk magmatism would have reached at least 4000 km^2; 2) extrusive volumes are larger than 8000 km^3; 3) it is volumetrically dominated (>75%) by dacite to rhyolite igneous rock that have calc-alkaline I-type signatures; 4) it is lithologically dominated by silicic ignimbrites; 5) igneous activity over long periods (> 30 Ma); and 6) a spatial and temporal relationship to continental rifting, plate break-up and potentially, other mafic large igneous provinces. The La Esperanza-Los Menucos magmatic system is not only temporally related to the Choiyoi magmatic province in western Argentina (Strazzere et al., 2006; Kleiman and Japas, 2009; Rocha Campos et al., 2011; Sato et al., 2015; Rocher et al., 2016), but also spatially associated with other late Permian to Triassic magmatic igneous complexes in Patagonia such as the Mamil Choique complex, Navarrete plutonic complex, Ramos Mejía and Yaminué igneous complexes (see Pankhurst et al., 2006, 2014; Martínez Dopico et al., 2011, 2017a). Further studies of the plutonic connections of the Choiyoi magmatic event and contemporaries should be focused on isotope, whole-rock and mineral geochemistry in order to understand the triggering factors for this regional magmatism.

FINAL REMARKS

La Esperanza plutonic-volcanic complex (LEPVC) and its temporal-lithological eruptive counterpart, the Los Menucos Group, meet the requirements for a Silicic Large Igneous Province (albeit rather smaller than most global examples) that is bracketed in age between 273 and 244 Ma. Several compositionally and isotopically distinct, high-K, magnesian, calc-alkaline series were distinguished: High Ba-Sr (i) metaluminous amphibole-biotite bearing granodiorites (273 ± 2 Ma); (ii) biotite and muscovite-bearing rhyolites and granites (265 ± 2 Ma; 260±2 Ma) and (iv) and metaluminous mafic microgranular enclave-bearing amphibole-biotite monzogranites (255 ± 2 Ma), dacites (253 ± 2 Ma), and slightly peraluminous granites; and, finally, Low Ba-Sr high silica metaluminous rocks (granites and acid dike swarms 250 ±2 Ma and ≈244 ± 2 Ma represented by the subvolcanic Calvo Granite and the acidic dike swarm. The episode of shallow intermediate to acidic granite magmatism in LEPVC is now dated with the new U-Pb SHRIMP zircon data for the Giménez Granite as old as 251 ± 2 Ma. Geochemistry revealed a multi-sourced open magmatic system evidenced by rocks with very different major and trace element contents and initial Sr and Nd ratios at equivalent SiO_2 intervals. The magmatic system underwent mafic magma replenishment (shown by the La Esperanza granodiorites and their mafic microgranular enclaves and the Collinao dacites) following an episode of crust-derived magmas represented by the Donosa granites and the Pailemán rhyolites. Available crystallization ages suggest the magmatism spanned in time over 30 Ma with two magmatic lulls (Fig. 10) that coincided with exhumation in upper crustal levels.

The new temporal, lithological, isotopic and geochemical features allow correlation of the La Esperanza plutonic-volcanic complex with the Los Menucos Group, encompassing a volume of magmatism comparable to a small-sized Silicic Large Igneous Province (Fig. 10). The mid–late Permian to Middle Triassic rocks in northern Patagonia record a transition between subduction-related magmatism (>273 Ma) associated with mafic magmatic sources with limited interaction with a felsic component, to post-orogenic extensional, mostly felsic hybridized sources (<260 Ma) in the Gondwana margin. Even though La Esperanza – Los Menucos magmatism would be coeval with the collision of the Patagonia terrane, syn-collisional magmatism or associated deformation were not found in upper crustal levels, as expected. However, the different nature and melting conditions of the inferred sources of the magmas that crystallized before 270 Ma, between 265 and 260 Ma, and from 255 to 245 Ma, suggest that the La Esperanza plutonic-volcanic complex was assembled during a 30 Ma period of major plate reorganization.

ACKNOWLEDGEMENTS

This work was supported by the Agencia Nacional de Investigaciones Científicas y Técnicas (Argentina) under grants PICT2013-1162 and PICT2016-2188, PICT2016-3148. We thank an anonymous reviewer and R. Pankhurst for thorough and constructive reviews and A. Folguera for his editorial handling. C.I. Martínez Dopico would like to thank T. Luppo, G. Giordanengo, and Fundaleu (Fundación de Lucha contra la Leucemia).

REFERENCES

Bea, F. 1996. Residence of REE, Y, Th and U in Granites and Crustal Protoliths; Implications for the Chemistry of Crustal Melts. Journal of Petrology 37(3):521-552 https://doi.org/10.1093/petrology/37.3.521

Black, L.P., Kamo, S.L., Allen, C.M., Aleinikoff, J.N., Davis, D.W., Korsch, R.J. and Foudoulis, C. 2003. TEMORA 1: a new zircon standard for Phanerozoic U-Pb geochronology. Chemical Geology 200:155-170.

Bouvier, A., Vervoort, J.D. and Parchett, P.J. 2008. The Lu-Hf and Sm-Nd isotopic composition of CHUR: Constraints from unequilibrated chondrites and implications for the bulk composition of terrestrial planets. Earth and Planetary Science Letters 273:48-57

Boynton, N.V. 1984. Cosmochemistry of the rare earth elements: meteorite studies. En Rare Earth Element Geochemistry (Henderson, P; editor). Development in Geochemistry 2: 63-114. Elsevier.

Bryan SE, Riley TR, Jerram DA, Leat PT, Stephens CJ (2002) Silicic volcanism: an under‐valued component of large igneous provinces and volcanic rifted margins. In: Menzies MA, Klemperer SL, Ebinger CJ, Baker J (eds) Magmatic Rifted Margins. Geological Society of America Special Paper, 362: 99‐120.

Caminos, R., Llambías, E.J., Rapela, C.W. and Párica, C.A. 1988. Late Paleozoic-Early Triassic magmatic activity of Argentina and the significance of new Rb-Sr ages from northern Patagonia. Journal of South American Earth Science 1:137-145.

Castillo, P., Fanning, C.M., Pankhurst, R.J., Hervé, F. and Rapela, C.W. 2017. Zircon O- and Hf-isotope constraints on the genesis and tectonic significance of Permian magmatism in Patagonia. Journal of the Geological Society 10.1144/jgs2016-152

Chappell, B.W., and White, A.J.R., 1983. Granitoid types and their distributions in the Lachlan Fold Belt, southeastern Australia. Geological Society of Australia Memoir 159:21-34.

Chernicoff, C.J., Zappettini, E.O., Santos, J.O.S., Belousova, E., and McNaughton, N.J., 2013. Combined U-Pb SHRIMP and Hf isotope study of the Late Paleozoic Yaminué Complex, Río Negro province, Argentina. Implications for the origin and evolution of the Patagonia composite terrane. Geoscience Frontiers 4 (6): 37-56.

Clemens, J.D., Helps, P.A., Stevens, G., 2010. Chemical structure in granitic magmas – a signal from the source? Earth Env. Sci. Trans. R. Soc. Edinburgh 100(1-2): 159-172. doi: 10.1017/s1755691009016053

Clemens, J.D. and Stevens, G., 2012. What Controls Chemical Variation in Granitic Magmas? Lithos 134-135: 317-329, DOI: 10.1016/j.lithos.2012.01.001

Cingolani, C., Dalla Salda, L., Hervé, F., Munizaga, F., Pankhurst, R.J., Parada, M.A., and Rapela, C.W. 1991. The magmatic evolution of northern Patagonia; New impressions of pre- andean tectonics. Geological Society of America, Special Paper 265: 29-43.

Cucchi, R., Lema, H., and Busteros, A., 2001. Hoja Geológica 4169-II, Los Menucos. Provincia de Río Negro. Instituto de Geología y Recursos Minerales, Servicio Geologico Minero Argentino. Boletín 265, 67p. Buenos Aires.

Deckart, K.,Hervé, F., Fanning, M., Ramírez,V., Calderón, and Godoy, M., 2014. U–Pb geochronology and Hf–O isotopes of zircons from the Pennsylvanian Coastal Batholith, South- Central Chile. Andean Geology 41, 49–82. http://dx.doi.org/10.5027/andgeoV41n1-a03

Farina, F., Stevens, G., Gerdes, A., Frei, D., 2014. Small-scale Hf isotopic variability in the Peninsula pluton (South Africa): the processes that control inheritance of source 176Hf/177Hf diversity in S-type granites. Contributions to Mineralogy and Petrology 168: 1065. https://doi.org/10.1007/s00410-014-1065-8

Fanning, C.M., Hervé, F., Pankhurst, R.J., Rapela, C.W., Kleiman, L.E., Yaxley, G.M. and Castillo, P. 2011. Lu–Hf isotope evidence for the provenance of Permian detritus in accretionary complexes of western Patagonia and the northern Antarctic Peninsula region. Journal of South American Earth Sciences, 32: 485–496.

Frost, B. R., Barnes, C. G., Collins, W. J., Arculus, R. J., Ellis, D. J. and Frost, C. D., 2001. A geochemical classification for granitic rocks. Journal of Petrology 42: 2033–2048.

Giacosa, R.E., Lema, H., Busteros, A., Zubia, M., Cucchi, R., and Tommaso, D.I., 2007. Estructura del Triásico de la región norte Macizo Nordpatagónico (40º-41ºS, 67º30´-69º45´O) Río Negro. Rev. Asoc. Geol. Argent. 62 (3): 355-365.

González, S.N., Greco, G.A., Sato, A.M., Llambías, E.J., Basei, M.A.S, González, P.D., Días, P.E., 2017. Middle Triassic trachytic lava flows associated with coeval dyke swarm in the North Patagonian Massif: A postorogenic magmatism related to entensional collapse of the Gondwanide orogen. Journal of South American Earth Sciences 75:134-143

Greco, G.A., González, P.D., González, S.N., Sato, A.M., Basei, M.A.S., Tassinari, C.C.G., Sato, K., Varela, R., and Llambías, E.J., 2015. Geology, structure and age of the Nahuel Niyeu Formation in the Aguada Cecilio area, North Patagonian Massif, Argentina. J.S.Am.Earth Sci. 62: 12-32. doi: 10.1016/j.jsames.2015.04.005.

Harris, N.B.W. and Pearce, J.A., and Tindle, A.G., 1986. Geochemical characteristics of collision- zone magmatism. In: Coward M P, Ries A C (eds) Collision Tectonics. Geological Society London Special Publication 19, pp 67-81.

Janousek V., Farrow C. M. and Erban V., 2006. Interpretation of whole-rock geochemical data in igneous geochemistry: introducing Geochemical Data Toolkit (GCDkit). Journal of Petrology 47(6): 1255-1259. doi: 10.1093/petrology/egl013

Janousek, V., Moyen, J.F., Martin, H., Erban, V., and Farrow, C., 2016. Geochemical Modelling of Igneous Processes – Principles and Recipes in R Language. Bringing the Power of R to a Geochemical Community. Springer-Verlag, Berlin, Heidelberg, pp 1–346

Kleiman, L.E. and Japas, M.S., 2009, The Choiyoi volcanic province at 34°-36°S (San Rafael, Mendoza, Argentina): implications for the late Paleozoic evolution of the southwestern margin of Gondwana: Tectonophysics 473: 283-299

Labudía, C.H. and Bjerg, E:A. 1994. Geología del Sector Oriental de la Hoja Bajo Hondo (39e), Provincia de Río Negro. Revista de la Asociación Geológica Argentina 49(3/4): 284-296.

Llambías, E.J and Rapela, C.W. 1984. Geología de los complejos eruptivos del Paleozoico superior de La Esperanza, provincia de Río Negro. Revista de la Asociación Geológica Argentina 39(3-4): 220-243.

Lucassen, F., Trumbull, R., Franz, G., Creixell, C., Vásquez, P., Romer, R.L., and Figueroa, O., 2004. Distinguishing crustal recycling and juvenile additions atactive continental margins: the Paleozoic to recent composition of the ChileanPacific margin (36-41ºS). Journal of South American Earth Sciences 17: 103-119

Ludwig, K.R. 2005. ISOPLOT/Ex A geochronological toolkit for microsoft excel. Berkeley Geochronology Center Special Publication Nº1a. Berkeley

Luppo, T., López de Luchi, M.G., Rapalini, A.E., Martínez Dopico and C.I., Fanning, C.M., 2018. Geochronologic evidence of a large magmatic province in northern Patagonia encompassing the Permian-Triassic boundary. Journal of South American Earth Sciences 82:346-355.

Luppo, T., Martínez Dopico, C.I., Rapalini, A.E., López de Luchi, M.G., Miguez, M., and Fanning, C.M., 2019. Paleomagnetism of Permo-Triassic volcanic units in northern patagonia: are we tracking the final stages of collision of Patagonia? International Journal of Earth Sciences 108(2):621-647

Martínez Dopico, C., Lopez de Luchi, M., Rapalini, A.E., and Kleinhanns, I.C. 2011. Crustal segments in the North Patagonian Massif, Patagonia: An integrated perspective based on Sm/Nd isotope systematics. Journal of South American Earth Sciences 31 : 324–341.

Martínez Dopico, C.I., López de Luchi, M.G. and Rapalini, A.E. 2014. Geoquímica del Complejo Plutónico La Esperanza (Pérmico), Provincia de Río Negro. XIX Congreso Geológico Argentino, Actas electrónicas S21-35, 2p., Córdoba, Argentina.

Martínez Dopico, C.I., López de Luchi, M.G., Wemmer, K., and Rapalini, A.E., 2013a. Composición química de biotita y hornblenda y edades de enfriamiento como indicadores de las condiciones de emplazamiento del Complejo Plutónico La Esperanza (Pérmico Superior), Macizo Norpatagónico. Revista de la Asociación Geológica Argentina 70: 3-15.

Martínez Dopico, C.I., Rapalini, A.E., López de Luchi, M.G., and Wemmer, K. 2013b. Assembly of shallow instrusions from multiple magma pulses in La Esperanza Plutonic Complex, Northpatagonian Massif, Argentina. LATINMAG LETTERS 3, OB06, 5p.

Martínez Dopico, C.I., López de Luchi, M.G., and Rapalini, A.E. 2014. Geoquímica del Complejo Plutónico La Esperanza (Pérmico), Provincia de Río Negro. XIX Congreso Geológico Argentino, Abstracts S21-35, Córdoba.

Martínez Dopico, C.I., López de Luchi, M.G., Rapalini, A.E., Wemmer, K., Fanning, M. and Basei., M. 2017a. Emplacement and temporal constraints of the gondwanan intrusive complexes of Northern Patagonia: La Esperanza plutono-volcanic case. Tectonophysics 712-713: 249-269 DOI: 10.1016/j.tecto.2017.05.015

Martínez Dopico, C.I., Tohver, E., López de Luchi, M.G., Wemmer, K., Rapalini, A.E., and Cawood, P.A., 2017b. Jurassic cooling ages in Paleozoic to early Mesozoic granitoids of northeastern Patagonia: 40Ar/39Ar, 40K-40Ar mica and U-Pb zircon evidence. Int. J. Earth Sci. Doi: 10.1007/s00531-016-1430-0.

Martínez Dopico, C., López de Luchi, M., Rapalini, A.E., Hervé, F., Fuentes, F., Fanning, M., 2017c. U-Pb SHRIMP dating of detrital zircon grains of the Colo Niyeu Formation: Extending the Neoproterozoic to Early Cambrian basins to central western northern Patagonia. XX Congreso Geológico Argentino, Tucumán 6 p

Middlemost, E. A. K. (1994). Naming materials in the magma/igneous rock system. Earth-Sciences Reviews 37, 215–224

Ohta, T and Arai, H., 2007. Statistical empirical index of chemical weathering in igneous rocks. Chemical Geology 18:280-297

Pankhurst, R.J., Rapela, C.W., Caminos, R., Llambías, E., and Parica, C., 1992. A revised age for the granites of the central Somuncura Batholith, North Patagonian Massif. Journal of South American Earth Sciences 5(3/4): 321-325.

Pankhurst, R., Leat, P., Sruoga, P., Rapela, C., Marquez, M., Storey, B. and Riley, T. 1998. The Chon Aike province of Patagonia y related rocks in West Antartica: a silicic large igneous province. Journal of Volcanology and Geothermal Research 81: 113-136.

Pankhurst, R.J., Riley, T.R., Fanning, C.M. and Kelley, S.P. 2000. Episodic silicic volcanism in Patagonia y the Antartic Peninsula: Chronology of magmatism associated with the break-up of Gondwana. Journal of Petrology 41: 605-625.

Pankhurst, R.J., Rapela, C.W., Fanning, C.M., and Márquez, M., 2006. Gondwanide continental collision and the origin of Patagonia. Earth-Science Rev. 76, 235–257. doi:10.1016/j.earscirev.2006.02.001

Pankhurst, R.J., Rapela, C.W., Lopez De Luchi, M.G., Rapalini, A.E., Fanning, C.M. and Galindo, C., 2014. The Gondwana connections of northern Patagonia. J. Geol. Soc. 171, 313e328. http://dx.doi.org/10.1144/jgs2013-081.

Paterson, S.R., Vernon, R.H., and Zak, J., 2005. Mechanical Instabilities and physical accumulation of K-feldspar megacrysts in granitic magma, Toulumne Batholith, California, USA. Journal of the Virtual Explorer 18, 1.

Peccerillo, A. and Taylor, S.R., 1976. Geochemistry of Eocene Calc-Alkaline Volcanic Rocks from the Kastamonu Area, Northern Turkey. Contributions to Mineralogy and Petrology 58: 63-81. http://dx.doi.org/10.1007/BF00384745Pearce, J. A., Harris, N. W. & Tindle, A. G., 1984. Trace element discrimination diagrams for the tectonic interpretation of granitic rocks. Journal of Petrology 25, 956–983.

Pearce, J. A., 1996. Sources and settings of granitic rocks. Episodes, Vol. 19, No. 4, p. 120-125.

Ramos, V.A., 1984 Patagonia: ¿Un continente paleozoico a la deriva? 9° Congreso Geológico Argentino, San Carlos de Bariloche, Actas 2, 311-325.

Rapela, C.W. and Llambías, E.J. 1985. Evolución magmática y relaciones regionales de los Complejos Eruptivos de La Esperanza, provincia de Río Negro. Revista de la Asociación Geológica Argentina 40(1-2): 4-25.

Ridolfi, F., and Renzulli, A., 2012. Calcic amphiboles in calc-alkaline and alkaline magmas: Thermobarometric and chemometric empirical equations valid up to 1130 °C and 2.2 GPa. Contributions to Mineralogy and Petrology, 163, 877–895.

Ridolfi, F., Renzulli, A., and Puerini, M., 2010. Stability and chemical equilibrium of amphibole in calc-alkaline magmas: An overview, new thermobarometric formulations and application to subduction-related volcanoes. Contributions to Mineralogy and Petrology, 160, 45–66

Roberts, M. and Clemens, J.D. 1993. Origin of high-potassium, calc-alkaline, I-type granitoids. Geology 21:825-828

Rocha-Campos, A.C., Basei, M.A., Nutman, A.P., Kleiman, L.E., Varela, R., Llambías, E., Canile, F.M., da Rosa, O., and de C.R., 2011, 30 million years of Permian volcanism recorded in the Choiyoi igneous province (W Argentina) and their source for younger ash fall deposits in the Paraná Basin: SHRIMP U-Pb zircón geochronology evidence: Gondwana Research, 19, 509-523

Rocher, S., Vallecillos, G., Castro de Machuca, B., and Alasino, P. 2015. El Grupo Choiyoi (Pérmico temprano-medio) en la Cordillera Frontal de Calingasta, San Juan, Argentina: volcanismo de arco asociado a extensión. Revista Mexicana de Ciencias Geológicas. 32(3):451-432.

Rotenberg, E., Davis, D.W., Amelin, Y., Ghosh, S., and Bergquist, B.A., 2012.Determina-tion of the decay-constant of ^{87}Rb by laboratory accumulation of ^{87}Sr. Geochimica Cosmochimica Acta 85: 41–57.

Sato, A.M., Llambías, E.J., Basei, M.A.S., and Castro, C.A., 2015, Three stages in the Late Paleozoic to Triassic magmatism of southwestern Gondwana, and the relationships with the volcanogenic events in coeval basins. Journal of South American Earth Sciences 63: 48-69

Solé, J., 2009, Determination of K-Ar ages in milligram samples using an infrared laser for argon extraction: Rapid Communications in Mass Spectrometry, v. 23, p. 3579–3590, doi: 10.1002 /rcm .4280.

Solé, J., and Enrique, P., 2001, X-ray fluorescence analysis for the determination of potassium in small quantities of silicate minerals for K-Ar dating: Analytica Chimica Acta, v. 440, p. 199–205, doi: 10 .1016 /S0003 -2670 (01)01060 -1

Strazzere, L., Gregori, D.A., and Dristas, J.A., 2006. Genetic evolution of PermoTriassic volcaniclastic sequences at Uspallata, Mendoza Precordillera, Argentina: Gondwana Research, 9, 485-499

Tarney, J. and Jones, C.E., 1994. Trace element geochemistry of orogenic igneous rocks and crustal growth models. Journal of the Geological Society, 151: 855-868.

Taylor, S.R. and McLennan, S.M., 1995. The geochemical evolution of the continental crust. Reviews in Geophysics 33: 241-265

Villaros, A., Stevens, G., Moyen, J.-F., Buick, I.S., 2009. The trace element compositions of S-type granites: Evidence for disequilibrium melting and accesory phase entrainment in the source. Contributions to Mineralogy and Petrology 158(4):543-561

Valley, J.W. 2003. Oxygen isotopes in zircon- Reviews in Mineralogy and Geochemistry 53(1) DOI :10.2113/0530343

Watson, E.B. and Harrison, T.M., 1983. Zircon saturation revisited: temperature and composition effects in a variety of crustal magma types. Earth Planetary Sciences Letters 64:295–304.

Williams, I.S., 1998, U-Th-Pb Geochronology by Ion Microprobe, en McKibben, M.A., Shanks III, W.C., Ridley, W.I. (eds.), Applications of microanalytical techniques to understanding mineralizing processes: Littleton, Society of Economic Geologists. Reviews in Economic Geology, 7: 1-35.

CAPTIONS

Figure 1 a) Location of the North Patagonian Massif in Northern Patagonia; b) Geological map of the La Esperanza area and surroundings. The yellow stars indicate the localities that were dated, as either U-Pb zircon SHRIMP dates or mica K-Ar cooling ages, whereas the black stars show the localities dated in this paper.

Figure 2 Plutonic units of the LEPVC a) Prieto Granodiorite at locality 19G 539094 m E, 5524100 m S, note the absence of enclaves; b) Plagioclase porphyritic magmatic microgranular enclave in La Esperanza granodiorites at 539934 m E, 5521493 m S; c) Giménez Granite (equigranular texture) in the locality type, nearby puesto Giménez (536362 m E, 5519878 m S); d) Megacrystic facies of Giménez granites in the locality dated herein (534601 m E, 5525913 m S). Donosa Granite and Calvo Granite are not shown here; the reader is referred to Martínez Dopico et al. (2017a).

Figure 3 a) Banded rhyolite from the top of the of the rhyolite dome; b) Syn-sedimentary folding in the Llanquil Formation; c) Collinao porphyritic dacite; d) Coarse-grained leucocratic Calvo granites in the sourroundings of puesto Calvo (see figure 1b).

Figure 4 U-Pb zircon dating of the Giménez Granite a) Cathodoluminescence images of the dated zircons. Note the inherited crystal-cores and dissolved areas; b) U-Pb concordia plot; c) Weighted average U^{238}-Pb^{206} (SHRIMP) crystallization age for Giménez Granite. A summary of the analytical data is in Table 2.

Figure 5 Major element geochemistry of the La Esperanza plutonic-volcanic complex (this paper; Rapela and Llambías, 1985). a) Binary diagram of (K_2O+Na_2O) vs SiO_2 (Middlemost, 1994) shows that most units follow a wide high K- calc-alkaline trend. The black and white stars represent average I- and S-type granite compositions reported by Chappell and White (1983) whereas fields a, b and c show the trends of differentiation of three examples of plutonic magma series: transitional, calc-alkaline and high-K rocks, respectively shown as in Roberts and Clemens (1983); b) Binary modified-alkali-lime index (Frost et al., 2011) vs SiO_2; note that the Prieto, La Esperanza, Giménez, Donosa and Collinao units extend over the calc-alkalic and calcic fields whereas Calvo Granite and some acidic dikes belong to the alkali-calcic to calc-alkalic domains; c) Alumina saturation indexes Al_2O_3/[(CaO+Na_2O+K_2O)- (1.67*CaO)] vs. Al_2O_3/(Na_2O+K_2O) (mol. %); and d) Sr-Rb-Ba Ternary diagram showing high and low Ba-Sr groups.

Figure 6. Major element (wt%) variation diagrams versus SiO_2 for entire chemical data set of the granitoid and volcanic groups. Yellow and pink lines indicate suggested evolutionary trends of low and high Sr-Ba groups, respectively.

Figure 7 Selected trace elements (Sr, Y, Rb, Ba, Ce, Zr; ppm) versus SiO_2 variation diagrams for the entire chemical data set of the granitoid and volcanic groups.

Figure 8 Chondrite-normalized REE patterns normalized to values of Boynton (1984) (left) and Spider plot of values normalized to the Upper Continental Crust of Taylor and McLennan (1995) (right).

Figure 9 Initial $^{87}Sr/^{86}Sr$ ratio vs SiO_2 of the units of the La Esperanza plutonic-volcanic complex. Data from the INGEIS data repository, Pankhurst et al. (1992, 2006), and Cingolani et al. (1991) were recalculated at the crystallization ages using the ^{87}Rb decay constant of Rotenberg et al. (2012). Data table as supplementary material and symbols as in figure 7.

Figure 10. Chronostratigraphic chart of the intrusive and extrusive rocks of La Esperanza, Los Menucos (25 km to the south of La Esperanza), Yaminué (100 km to the East) and Sierra Grande areas (250 km to the East), showing crystallization (U-Pb zircon) and cooling (K-Ar and Ar-Ar mica)

ages (Pankhurst et al., 2006, 2014; Chernicoff et al., 2013; Martínez Dopico, 2017a,b,c; Luppo et al., 2018, 2019; González et al., 2014, this paper), and isotope parameters (Pankhurst et al., 2006; Castillo et al., 2017). Note the similarity of the crystallization-time intervals of the plutonic rocks.

Table 1. Summary of zircon crystallization ages (U-Pb SHRIMP) and biotite/white mica cooling ages in the La Esperanza area. References: P92, P06- Pankhurst et al. (1992, 2006); C13, C17, C19- Martínez Dopico et al. (2013, 2017a, c); L18, L19 -Luppo et al. (2018, 2019).

Table 2. Summary of the U-Pb SHRIMP results of sample Z9 of Giménez Granite.

Table 3. Summary of the K-Ar results of muscovite of samples Z67 (Donosa Granite) and D35 (Ms-bearing leucogranite dike).

Table 4. Typical whole-rock major and trace elements geochemical data of several units of the La Esperanza plutonic-volcanic complex.

Table 5. Initial $^{87}Sr/^{86}Sr$ ratios from the IR INGEIS data repository, P92 Pankhurst et al. (1992, 2006) and C92 Cingolani et al. (1991) have been recalculated at their respective zircon U-Pb crystallization age and using the ^{87}Rb decay constant of Rotenberg et al. (2012).

Supplementary material

Table 6 Chemical composition of plagioclase crystals of Prieto Granodiorite, La Esperanza Monzogranite, and Donosa Granite. EPMA measurement conditions and procedures are explained in Martínez Dopico et al. (2013).

PETROGRAPHIC APPENDIX

Sample Z9 (biotite-bearing megacrystic granite): Location: 40 ° 25.011'S 68 ° 35.536'W

Macroscopically, it is an orange pink color rock with a banded structure and fine to very fine texture very inhomogeneous in which eventual larger crystals of potassium feldspar of tabular pink color that can reach very sporadically up to 12 cm (0.4 cm average) and to a lesser extent and size, tabular crystals of white plagioclase of somewhat larger size over a granite composition matrix with biotite. The textural inhomogeneity is given by the presence of laminar sectors of up to 6 cm of maximum thickness composed macroscopically by black biotite crystals.

The rock has a banded structure where lighter bands of granitic composition dominate over irregular dark bands (schlieren). The dark schlierens are coherent bands composed of aggregates of pleochroic biotite lamellae of dark yellow chestnut of different sizes and riddled with zircon inclusions with pleochroic halo development. Within these bands, large euhedral crystals of pleochroic andalusite with a thin crown of imbalance of muscovite, which is in contact with the biotite, can be distinguished. Another mineral that is inside the schlieren is cordierite. It exhibits equidimensional shapes completely replaced by a radial aggregate of green chlorite and clays. Interstitially in these minerals, there are quartz crystals. The lightest sector of the rock is of granitic composition with an equigranular subidiomorphic texture to a slightly unequal shape given by the presence of sporadic crystals of somewhat larger size of K-feldspar associated with somewhat smaller crystals also of k-feldspar, plagioclase, quartz, biotite, muscovite, apatite and zircon.

The biotite strips or schlieren are composed of biotite, andalusite, muscovite, opaque minerals, quartz, cordierite and plagioclase. The sub to euhedral biotite lamellae are the most abundant component of the fringes, surround the andalusite crystals and generate a mosaic in which the interstices are arranged in subhedral crystals to anhedral crystals of plagioclase and quartz. Opaque minerals are very scarce (<1%) and are represented by magnetite incipiently replaced by hematite (martitization).

Crystal	Area	SiO2	Al2O3	CaO	BaO	Na2O	K2O	FeO	Total	%An
Prieto Granodiorite										
Pl1	Inner core	57.2	27.45	9.68	0.0953	6.59	0.1532	0.1225	101.29	45
Pl1	Outer core	57.39	27.02	9.25		6.76	0.1169	0.1057	100.64	44
Pl1	Rim	62.51	24.27	5.43	0	8.66	0.2026	0.1803	101.26	24
Pl1	Rim	61.96	24.22	5.46	0.0017	8.44	0.2833	0.1803	100.54	26
Pl2	Inner core	54.58	28.96	10.38	0.0381	5.51	0.196	0.1814	99.85	55
Pl2	Inner core	57.62	27.04	8.71	0.0347	6.51	0.2029	0.167	100.29	43
Pl2	Outer core	59.03	25.94	8.06	0.0277	7.25	0.2248	0.113	100.65	38
Pl2	Rim	62.89	23.92	5	0	8.93	0.1649	0.0529	100.96	22
Donosa Granite										
Pl1	Inner core	63.25	22.11	3.36		9.85	0.12	0.018	98.71	21
Pl1	Outer core	62.27	23.64	4.86	0.119	9.06	0.1591	0.0504	100.16	25
Pl1	Rim	64.16	22.77	3.3	0.0207	9.71	0.2436	0.024	100.24	18
Pl2	Core	61.64	23.89	4.89	0.0138	8.75	0.3343		99.52	28
Pl2	Core	61.76	23.57	4.85	0.045	8.54	0.3221	0.0288	99.12	27
Pl2	Rim	64.68	22.88	3.4		9.96	0.1722	0.3329	101.43	16
La Esperanza Monzogranite										
Pl1	Core	58.27	26.38	8.04	0.0572	6.78	0.2229	0.2235	99.97	41
Pl1	Core	59.12	26.03	7.51	0.0537	7.36	0.2278	0.215	100.53	38
Pl1	Core	57.1	26.34	8.35	0.1178	6.76	0.3255	0.2775	99.29	46
Pl1	Rim	62.61	22.95	4.95	0	8.93	0.3287	0.1082	99.87	24
Pl1	Rim	63.16	22.93	4.15	0	9.1	0.4261	0.1335	99.9	22
Pl2	Core	59.6	25.7	8.17	0	7.07	0.1637	0.1671	100.88	36
Pl3	Core	59.37	25.33	7	0.0104	7.78	0.3021	0.2129	100.01	37
Pl3	Core	59.7	26.01	7.17	0	7.37	0.1627	0.1694	100.58	35
Pl3	Rim	62.41	23.01	5.05	0	8.94	0.3274	0.1092	99.85	25
Pl3	Core	59.27	25.53	7	0.0104	7.68	0.3032	0.2119	100.01	37

	Sample	Lithology	Method	Material	Reference	Interpretation			Observation
Cambrian Metamorphic Basement									
							MDA		
Colo Niyeu Fm	Z316	Sandstone, Quartzite Mb	U-Pb SHRIMP	Zrc	C19	*MDA*	***530***	Depo age *528+-2 Ma*	
La Esperanza Plutono- Volcanic Complex							**Age (Ma)**	**±**	
Prieto Granodiorite	LES-118	Equigranular Bt-Amp Granodiorite	U-Pb SHRIMP	Zrc	P06	*Crystallization*	**273**	**2**	
	Z6	Equigranular Bt-Amp Granodiorite	K-Ar	Bio	C13	*Cooling at 300ºC*	**259**	**6**	Next to the contact with Donosa Granite
Pailemán Rhyolite	LES-125	Rhyolite	U-Pb SHRIMP	Zrc	P06	*Crystallization*	**265**	**2**	
Donosa Granite	Z67	Megacrystic Granite	U-Pb SHRIMP	Zrc	C17	*Crystallization*	**260**	**2**	
	-	Megacrystic Granite	Rb-Sr	WR	P92	*Cooling at 500ºC*	**259**	**15**	
	Z67-b	Megacrystic Granite	K-Ar	Ms	C17	*Cooling at 450ºC*	**265**	**3**	
	Z12	Megacrystic Granite	K-Ar	Bio	C13	*Cooling at 300ºC*	**237**	**3**	Next to the contact with Calvo Granite
La Esperanza Monzogranite	Z20	Inequigranular Bt-Amp	U-Pb SHRIMP	Zrc	C17	*Crystallization*	**255**	**2**	
	Z20	Inequigranular Bt-Amp	K-Ar	Bio	C17	*Cooling at 300ºC*	**248**	**4**	
	Z287	Inequigranular Bt-Amp	K-Ar	Bio	C17	*Cooling at 300ºC*	**251**	**6**	
Collinao Dacite	E5	Rhyodacite	U-Pb SHRIMP	Zrc	*L19*	*Crystallization*	**253**	**2**	
Giménez Granite	Z9	Metatexite	U-Pb SHRIMP	Zrc	*this study*	*Crystallization*	**251**	**2**	
	-	Bt-Granite	Rb-Sr	WR	*P92*	*Cooling at 500ºC*	**258**	**8**	
	Z305b	Banded Granite	K-Ar	Bio	C17	*Cooling at 300ºC*	**232**	**4**	
Calvo Granite	LES-119	Leucogranite	U-Pb SHRIMP	Zrc	P06	*Crystallization*	**250**	**2**	*260* *290*
	-	Leucogranites	Rb-Sr	WR	P92	*Cooling at 500ºC*	**239**	**5**	
Acidic dike	D35a	Ms-granite	K-Ar	Ms	*this study*	*Crystallization*	**260**	**6**	
Acidic dike	LES-122	Volcanic rock with devi	U-Pb SHRIMP	Zrc	P06	*Crystallization*	**246**	**2**	
	DZ3	Fine grained Granite	U-Pb SHRIMP	Zrc	*L19*	*Crystallization*	**244**	**2**	

Table *2* . Summary of SHRIMP U-Pb results for zircon from sample Z9

Grain. spot	U (ppm)	Th (ppm)	Th/U	$^{206}Pb^*$ (ppm)	$^{204}Pb/^{206}Pb$	f_{206} %	Total $^{238}U/^{206}Pb$	1-s ±	Total $^{207}Pb/^{206}Pb$	1-s ±	Radiogenic $^{206}Pb/^{238}U$	1-s ±	Age (Ma) $^{206}Pb/^{238}U$	±	
1.1	456	170	0.37	15.7	-	0.01	24.90	0.27	0.0514	0.0008	0.0402	0.0004	253.8	2.8	*
2.1	513	230	0.45	17.3	0.000054	0.03	25.44	0.28	0.0514	0.0006	0.0393	0.0004	248.5	2.7	*
2.2	147	90	0.61	5.1	0.000436	0.94	24.59	0.32	0.0588	0.0022	0.0403	0.0005	254.6	3.3	*
3.1	694	348	0.50	24.3	0.000058	<0.01	24.48	0.27	0.0513	0.0005	0.0408	0.0004	258.1	2.8	
4.1	639	264	0.41	21.8	0.000059	0.08	25.18	0.27	0.0519	0.0005	0.0397	0.0004	250.9	2.7	*
5.1	423	419	0.99	14.2	-	<0.01	25.63	0.28	0.0510	0.0006	0.0390	0.0004	246.7	2.7	*
6.1	433	202	0.47	14.3	0.000101	<0.01	26.09	0.29	0.0510	0.0006	0.0383	0.0004	242.5	2.7	
7.1	443	284	0.64	15.0	-	<0.01	25.36	0.28	0.0512	0.0006	0.0394	0.0004	249.3	2.7	*
8.1	253	106	0.42	8.6	0.000277	<0.01	25.35	0.30	0.0505	0.0008	0.0395	0.0005	249.6	2.9	*
9.1	452	196	0.43	15.1	-	0.05	25.66	0.29	0.0515	0.0006	0.0390	0.0004	246.3	2.8	*
10.1	684	341	0.50	22.9	0.000008	0.10	25.66	0.28	0.0519	0.0005	0.0389	0.0004	246.2	2.7	*
11.1	718	511	0.71	24.2	-	0.04	25.44	0.27	0.0515	0.0005	0.0393	0.0004	248.4	2.6	*
12.1	585	251	0.43	20.4	0.000065	0.01	24.67	0.27	0.0514	0.0005	0.0405	0.0004	256.1	2.7	*
13.1	653	334	0.51	22.4	-	<0.01	25.03	0.27	0.0512	0.0005	0.0400	0.0004	252.6	2.7	*
14.1	2412	95	0.04	101.7	0.005337	*9.93*	20.38	0.21	0.1315	0.0011	0.0442	0.0005	278.8	2.9	
14.2	28	24	0.84	1.5	-	0.04	16.33	0.31	0.0546	0.0020	0.0612	0.0012	383	7	*Inheritance*
15.1	518	242	0.47	17.3	-	0.10	25.65	0.28	0.0519	0.0007	0.0390	0.0004	246.3	2.7	*
16.1	253	88	0.35	8.7	0.000008	<0.01	25.08	0.30	0.0506	0.0008	0.0399	0.0005	252.2	3.0	*
17.1	441	189	0.43	15.1	-	<0.01	25.03	0.28	0.0512	0.0006	0.0400	0.0004	252.6	2.8	*
17.2	288	150	0.52	9.8	-	0.02	25.15	0.29	0.0514	0.0007	0.0397	0.0005	251.3	2.9	*
18.1	438	163	0.37	15.0	-	<0.01	25.10	0.28	0.0509	0.0006	0.0399	0.0004	252.0	2.8	*
18.2	164	93	0.57	5.6	0.000113	0.28	25.08	0.32	0.0535	0.0010	0.0398	0.0005	251.3	3.1	*
19.1	802	669	0.83	27.6	-	<0.01	24.93	0.26	0.0510	0.0004	0.0401	0.0004	253.7	2.7	*
20.1	601	254	0.42	21.5	0.000024	<0.01	24.05	0.26	0.0512	0.0005	0.0416	0.0005	262.7	2.8	
20.2	198	149	0.75	7.0	-	<0.01	24.36	0.30	0.0507	0.0009	0.0411	0.0005	259.5	3.1	
21.1	353	145	0.41	12.3	0.000088	<0.01	24.63	0.28	0.0507	0.0008	0.0406	0.0005	256.8	2.9	*
22.1	736	364	0.50	25.7	0.000126	0.23	24.62	0.27	0.0532	0.0005	0.0405	0.0004	256.0	2.8	*

Age ± internal **± include std: ie external**

wtd ave dominant	**251.1**	1.5	0.72	**1.8**	MSWD = 1.4 for 21 of 27 areas analysed

Notes:
1. Uncertainties given at the one σ level.
2. Error in Temora reference zircon calibration was 0.41% for the analytical session.
   (not included in above errors but required when comparing data from different mounts).
3. f_{206} % denotes the percentage of common Pb (^{206}Pb)
4. Correction for common Pb for the U/Pb data has been made using the measured ^{238}U/^{206}Pb and ^{207}Pb/^{206}Pb ratios
   following Tera and Wasserburg (1972) as outlined in Williams (1998).

* Used for age calculation

Sample	Unit	Mineral	K_2O	^{40}Ar *	Age	2s-Error
			[Wt. %]	[%]	[Ma]	[Ma]
Z67b	Donosa Granite	Ms	8.41	98.3	259.6	5.8
D35a	Ms-Acid Dike	Ms	8.18	98.7	259.8	6.2

Sample	Z19	DZ3	LZ13	D55	D39	Z302	Z67	Z1
Locality	555273 E	552708 E	547571 E	552755 E	552977 E	546643 E	544311 E	549840 E
(UTM m 19G)	5506688 S	5523514 S	5535526 S	5521004 S	5532826 S	5525866 S	5527092 S	5515478 S
Lithology	porphyritic rhyolite	aphyric rhyolite	leucogranite	hb- bt Granite	rhyolite	dacite	megacrystic granite	bt-hb granodiori
Unit	acidic dike	acidic dike	Calvo Granite	La Esperanza Monzogranite	Paileman dome	Collinao Dacite	Donosa Granite	Prieto Granodiorite
SiO_2	69.52	78.60	75.89	69.20	74.20	60.06	74	64.08
Al_2O_3	14.42	12.00	12.28	14.70	14.10	16.88	14.29	15.09
Fe_2O_{3t}	3.56	2.15	0.73	3.97	1.97	6.02	1.89	5.41
MnO	0.06	0.02	0.08	0.07	0.03	0.05	0.029	0.075
MgO	1.20	0.02	0.11	1.21	0.37	2.41	0.43	2.22
CaO	2.41	0.26	0.62	2.85	1.31	4.78	1.72	3.73
Na_2O	3.74	3.27	3.87	3.52	3.34	3.73	3.99	3.42
K_2O	4.03	4.97	5.04	3.83	3.89	2.04	3.77	4.83
TiO_2	0.42	0.09	0.10	0.42	0.18	0.84	0.23	0.57
P_2O_5	0.13	0.01	0.01	0.13	0.03	0.23	0.09	0.15
LOI	1.10	0.12	0.46	0.58	0.89	2.16	0.7	0.86
Total	100.60	101.51	99.19	100.48	100.31	99.19	101.14	100.44
Sc	7	2	4	7	2	13	3	10
Be	2		6	n.d.	n.d.	3	3	3
V	62	57	9	64	19	137	20	99
Cr	20	20	20	20	10	20	20	30
Co	7	1	1	9	2	10	2	11
Ni	20	7	20	7	5	20	20	20
Cu	60	15	10	14	4	10	10	10
Zn	40	9	30	40	31	40	30	60
Ga	17	13.9	19	17.5	18	23	20	19
Ge	1	5	3	5	5	2	1	1
As	5	1.9	5	0.9	1.9	31	5	5
Rb	140	256	348	171.5	158	90	144	225
Sr	402	49.1	35	388	450	593	476	392
Y	14	17.9	17	18.6	8.7	24	6	18
Zr	146	88	80	136	109	204	112	173
Nb	12	18.5	29	15.8	9.4	14	9	11
Mo	2	2	2	1	1	2	2	2
Ag	0.5	0.5	0.5	0.5	0.5	1.1	0.5	0.5
In	0.2	0.006	0.2	0.014	0.005	0.2	0.2	0.2
Sn	3	3	4	3	2	5	2	4
Sb	0.5	0.2	0.5	0.14	0.71	1.3	0.5	0.5
Cs	2.2	1.71	6.9	8.33	9.12	4.5	3.1	9.1
Ba	1102	102.5	110	808	1110	542	913	800
La	38.4	32	22.4	42	24.6	41.9	24.4	50.3
Ce	73.6	59.2	42.3	77.5	46.1	87	47.4	99.1
Pr	7.47	5.42	3.87	8.17	4.91	9.76	4.95	10.1
Nd	26.1	15.8	11.4	27.7	17.7	36.7	17.2	34.8
Sm	4.5	2.58	1.9	4.66	2.66	6.8	3	6
Eu	0.93	0.29	0.2	0.95	0.49	1.35	0.58	1.13
Gd	3.1	2.05	1.5	3.34	1.79	5	1.8	4.2
Tb	0.5	0.4	0.3	0.54	0.29	0.8	0.3	0.6
Dy	2.7	2.24	1.9	3.02	1.48	4.3	1.3	3.3
Ho	0.5	0.56	0.4	0.61	0.29	0.8	0.2	0.6
Er	1.5	1.69	1.5	1.71	0.76	2.3	0.7	1.8
Tm	0.22	0.28	0.31	0.26	0.12	0.34	0.1	0.28

Yb	1.5	2.13	2.6	1.71	0.8	2.3	0.6	1.9
Lu	0.25	0.32	0.48	0.25	0.12	0.36	0.1	0.3
Hf	4.5	3.6	4	3.9	3.2	5.4	3.3	5.5
Ta	1.3	1.5	2.9	1.6	0.9	1.3	1.1	1.2
W	2	2	1	3	7	1	1	5
Tl	0.9	0.08	1.7	0.3	0.13	0.5	0.6	1.2
Pb	18	16	37	21	14	14	22	29
Bi	0.4	0.17	0.4	0.19	0.06	0.5	0.4	0.6
Th	14.6	25.6	33.3	19.1	9.11	23.6	8	28.5
U	4.6	2.28	5.5	3.28	2.11	5.8	1.9	7.6
Eu/Eu*	0.76	0.39	0.36	**0.74**	0.69	0.71	0.76	0.69
La/YbN	17.26	10.13	5.81	16.56	20.73	12.28	27.42	17.85
La/SmN	5.37	7.8	7.42	5.67	5.82	3.88	5.12	5.27
Sum REE	161.27	124.96	91.06	172.42	102.11	199.71	102.63	214.41

ite

Sample	Unit	Lithology	Crystalliza- tion Age	SiO_2	Sr	Rb	87Rb/86Sr	87Sr/86Sr	2S	εSr (WR)	Initial 87Sr/86Sr	Reference		εNd (WR)	Initial 143Nd/144Nd	Reference	εHf (Zrc)	δ18O‰	Reference
LES-125	Rhyolite dome	rhyolite	264	73.0	123	427	6.500	0.731292	n.d.	3.8	0.707275	P06		-5.8	0.511992	P06	`-3.8 to -8.7	`6.6 to 7.0	Ca17
LE 101	Rhyolite dome	rhyolite	264	70.9	167	394	6.8300	0.73450	.050	4.3	0.709264	IR							
LE 102	Rhyolite dome	rhyolite	264	70.8	171	473	6.4600	0.73230	.050	3.9	0.708431	IR							
LE 146	Rhyolite dome	rhyolite	264	73.0	193	171	2.4600	0.71610	.050	1.6	0.707011	IR							
LES-118	Calvo Granite	leucogranite	250	75.9	35	377	29.096	0.807041	n.d.	14.6	0.705246	P06		-7.5	0.511922	P06	`-5.6 to -9.0	`4.4 to 5.8	Ca17
LE 185	Calvo Granite	leucogranite	250	78.2	13.4	228	50.0800	0.87735	.015	24.5	0.702135	P92	*						
LE 126A	Calvo Granite	leucogranite	250	76.8	7.4	232	93.1900	1.01821	.020	44.5	0.692178	P92	*						
LE 126B	Calvo Granite	leucogranite	250	76.8	7.4	225	91.0400	1.01775	.020	44.5	0.699238	P92	*						
LE 127	Calvo Granite	leucogranite	250	77.3	15.8	241	44.6900	0.85906	.015	21.9	0.702704	P92	*						
LE 131	Calvo Granite	leucogranite	250	75.0	12.9	224	51.0300	0.88252	0.0150	25.3	0.703990	P92	*						
LE 132A	Calvo Granite	leucogranite	250	74.9	90.5	256	8.1990	0.73505	.010	4.3	0.706365	P92							
LE 132B	Calvo Granite	leucogranite	250	74.9	88.8	250	8.1680	0.73503	.010	4.3	0.706454	P92							
LES-120	Donosa Granite	granite	260	73.0	480	139	0.698	0.710168	n.d.	0.8	0.707628	P06		-9.8	0.511794	P06			
LE 120	Donosa Granite	granite	260	73.1	532	133	0.7249	0.71022	.010	0.8	0.707582	P92							
LE 121	Donosa Granite	granite	260	74.3	377	137	1.0554	0.71149	.010	1.0	0.707646	P92							
LE 134	Donosa Granite	granite	260	75.2	321	186	1.6788	0.71374	.010	1.3	0.707627	P92							
LE 137A	Gimenez Granite	granite	251	75.3	239	209	2.5378	0.71645	.010	1.7	0.707535	P92							
LE 137B	Gimenez Granite	granite	251	75.3	233	204	2.5420	0.71646	.010	1.7	0.707526	P92							
LE 139	Gimenez Granite	granite	251	71.4	475	153	0.9351	0.71056	.010	0.9	0.707275	P92							
LES-119	Prieto Granodiorite	granodiorite	273	67.0	440	161	1.065	0.710794	n.d.	0.9	0.706725	P06		-4.8	0.512033	P06	`-2.9 to -4.6	`6.0 to 7.3	Ca17
CON-88.48	Prieto Granodiorite	granodiorite	273	67.0	445	175	1.1390	0.71084	.010	0.9	0.706488	C91							
LE 165	Prieto Granodiorite	granodiorite	273	66.8	421	183	1.2570	0.71145	.010	1.0	0.706649	P92							
LE 169	Prieto Granodiorite	granodiorite	273	67.3	418	179	1.2384	0.71122	.010	1.0	0.706487	P92							
LE 152	Collinao Dacite	dacite	252	65.5	445	206	1.3000	0.71310	.050	1.2	0.708515	IR							
LE 99 A	La Esperanza Monzo	granodiorite	255	68.1	542	179	0.8688	0.71028	.010	0.8	0.707179	P92							
LE 99 B	La Esperanza Monzo	granodiorite	255	68.1	426	129	0.8731	0.71024	.010	0.8	0.707122	P92							
LE 130	La Esperanza Monzo	granite	255	71.8	323	164	1.4651	0.71224	.010	1.1	0.707006	P92							
LE 136	La Esperanza Monzo	monzogranite	255	70.9	429	102	0.6905	0.70969	.010	0.7	0.707226	P92							
465	La Esperanza Monzc	granodiorite	255	67.0	394	195	1.4333	0.71193	.010	1.1	0.706814	P92	*						
LES-122	Rhyolite dike	rhyolite	245	?													`-7.4 to -8.7	`5.1 to 6.6	Ca17

* not considered

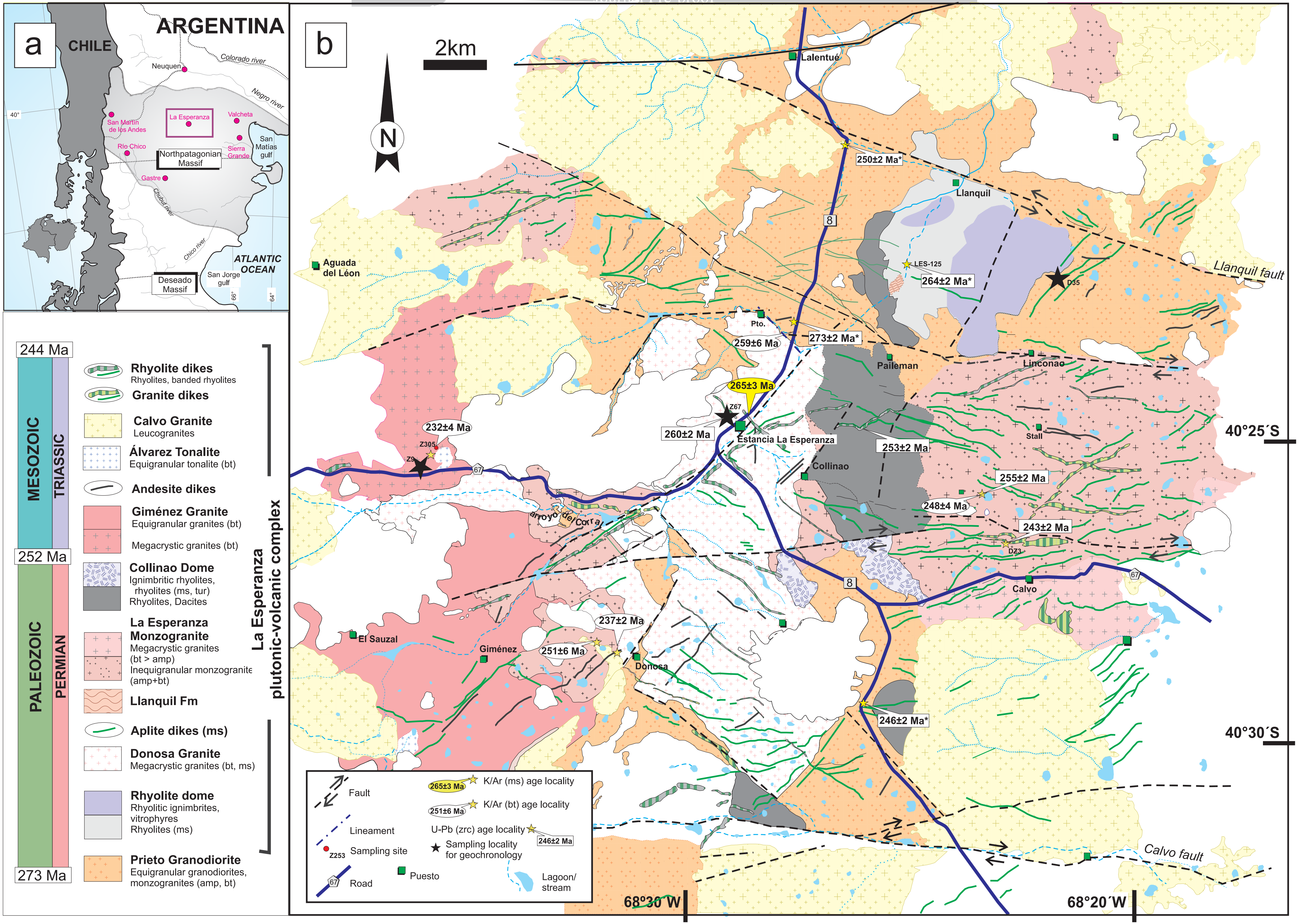
a
CHILE
ARGENTINA
Neuquen
Colorado river
Negro river
40°
San Martin de los Andes
La Esperanza
Valcheta
San Matías gulf
Rio Chico
Northpatagonian Massif
Sierra Grande
Gastre
Chubut river
Chico river
ATLANTIC OCEAN
San Jorge gulf
Deseado Massif
66°
64°
244 Ma
MESOZOIC
TRIASSIC
252 Ma
PALEOZOIC
PERMIAN
273 Ma
Rhyolite dikes
Rhyolites, banded rhyolites
Granite dikes
Calvo Granite
Leucogranites
Álvarez Tonalite
Equigranular tonalite (bt)
Andesite dikes
Giménez Granite
Equigranular granites (bt)
Megacrystic granites (bt)
Collinao Dome
Ignimbritic rhyolites, rhyolites (ms, tur)
Rhyolites, Dacites
La Esperanza Monzogranite
Megacrystic granites (bt > amp)
Inequigranular monzogranite (amp+bt)
Llanquil Fm
Aplite dikes (ms)
Donosa Granite
Megacrystic granites (bt, ms)
Rhyolite dome
Rhyolitic ignimbrites, vitrophyres
Rhyolites (ms)
Prieto Granodiorite
Equigranular granodiorites, monzogranites (amp, bt)
La Esperanza plutonic-volcanic complex
b
2km
N
Lalentue
250±2 Ma*
Llanquil
8
LES-125
264±2 Ma*
D35
Llanquil fault
Aguada del Léon
Pto.
259±6 Ma
273±2 Ma*
Paileman
Linconao
265±3 Ma
Z67
260±2 Ma
Estancia La Esperanza
253±2 Ma
Collinao
Stall
40°25´S
232±4 Ma
Z305
Z9
67
255±2 Ma
248±4 Ma
arroyo del Corral
243±2 Ma
DZ3
Calvo
237±2 Ma
El Sauzal
Giménez
251±6 Ma
Donosa
246±2 Ma*
40°30´S
Fault
Lineament
Z253 Sampling site
Road
265±3 Ma K/Ar (ms) age locality
251±6 Ma K/Ar (bt) age locality
U-Pb (zrc) age locality 246±2 Ma
Sampling locality for geochronology
Puesto
Lagoon/ stream
Calvo fault
68°30´W
68°20´W

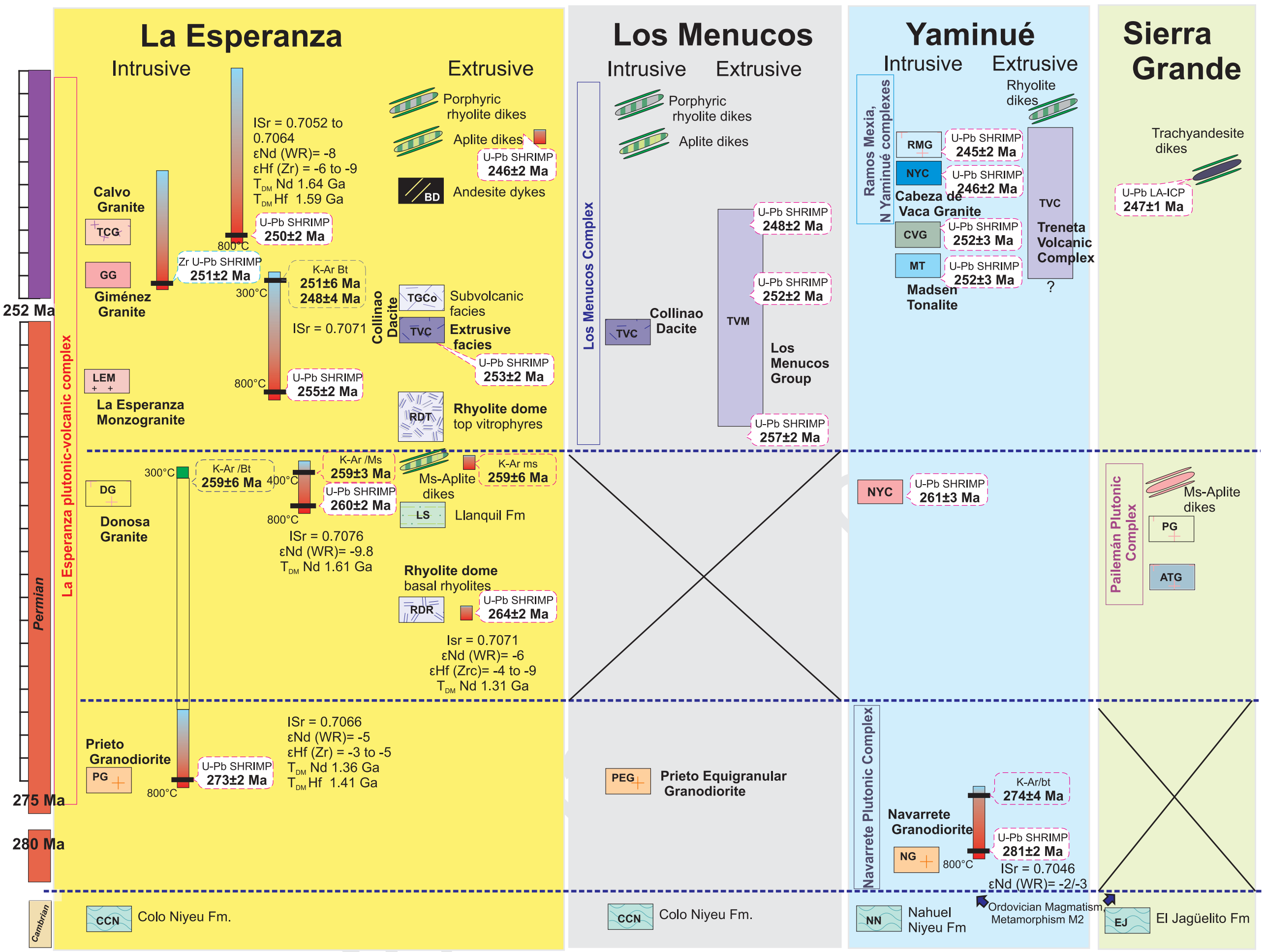
La Esperanza
Intrusive
Extrusive
La Esperanza plutonic-volcanic complex
Permian
Cambrian
252 Ma
275 Ma
280 Ma
Porphyric rhyolite dikes
Aplite dikes
U-Pb SHRIMP 246±2 Ma
BD
Andesite dykes
ISr = 0.7052 to 0.7064
εNd (WR)= -8
εHf (Zr) = -6 to -9
TDM Nd 1.64 Ga
TDM Hf 1.59 Ga
800°C
U-Pb SHRIMP 250±2 Ma
Calvo Granite
TCG
GG
Giménez Granite
Zr U-Pb SHRIMP 251±2 Ma
300°C
K-Ar Bt 251±6 Ma 248±4 Ma
ISr = 0.7071
Collinao Dacite
TGCo
Subvolcanic facies
TVC
Extrusive facies
U-Pb SHRIMP 253±2 Ma
800°C
U-Pb SHRIMP 255±2 Ma
LEM
La Esperanza Monzogranite
RDT
Rhyolite dome top vitrophyres
300°C
K-Ar /Bt 259±6 Ma
400°C
K-Ar /Ms 259±3 Ma
U-Pb SHRIMP 260±2 Ma
Ms-Aplite dikes
K-Ar ms 259±6 Ma
DG
Donosa Granite
800°C
LS
Llanquil Fm
ISr = 0.7076
εNd (WR)= -9.8
TDM Nd 1.61 Ga
Rhyolite dome basal rhyolites
RDR
U-Pb SHRIMP 264±2 Ma
Isr = 0.7071
εNd (WR)= -6
εHf (Zrc)= -4 to -9
TDM Nd 1.31 Ga
Prieto Granodiorite
PG
U-Pb SHRIMP 273±2 Ma
800°C
ISr = 0.7066
εNd (WR)= -5
εHf (Zr) = -3 to -5
TDM Nd 1.36 Ga
TDM Hf 1.41 Ga
CCN
Colo Niyeu Fm.
Los Menucos
Intrusive
Extrusive
Los Menucos Complex
Porphyric rhyolite dikes
Aplite dikes
U-Pb SHRIMP 248±2 Ma
U-Pb SHRIMP 252±2 Ma
TVM
TVC
Collinao Dacite
Los Menucos Group
U-Pb SHRIMP 257±2 Ma
PEG
Prieto Equigranular Granodiorite
CCN
Colo Niyeu Fm.
Yaminué
Intrusive
Extrusive
Ramos Mexia. N Yaminué complexes
Rhyolite dikes
RMG
U-Pb SHRIMP 245±2 Ma
NYC
U-Pb SHRIMP 246±2 Ma
Cabeza de Vaca Granite
CVG
U-Pb SHRIMP 252±3 Ma
MT
U-Pb SHRIMP 252±3 Ma
Madsen Tonalite
TVC
Treneta Volcanic Complex
?
NYC
U-Pb SHRIMP 261±3 Ma
Navarrete Plutonic Complex
K-Ar/bt 274±4 Ma
Navarrete Granodiorite
U-Pb SHRIMP 281±2 Ma
NG
800°C
ISr = 0.7046
εNd (WR)= -2/-3
Ordovician Magmatism, Metamorphism M2
NN
Nahuel Niyeu Fm
Sierra Grande
Trachyandesite dikes
U-Pb LA-ICP 247±1 Ma
Pailemán Plutonic Complex
Ms-Aplite dikes
PG
ATG
EJ
El Jagüelito Fm

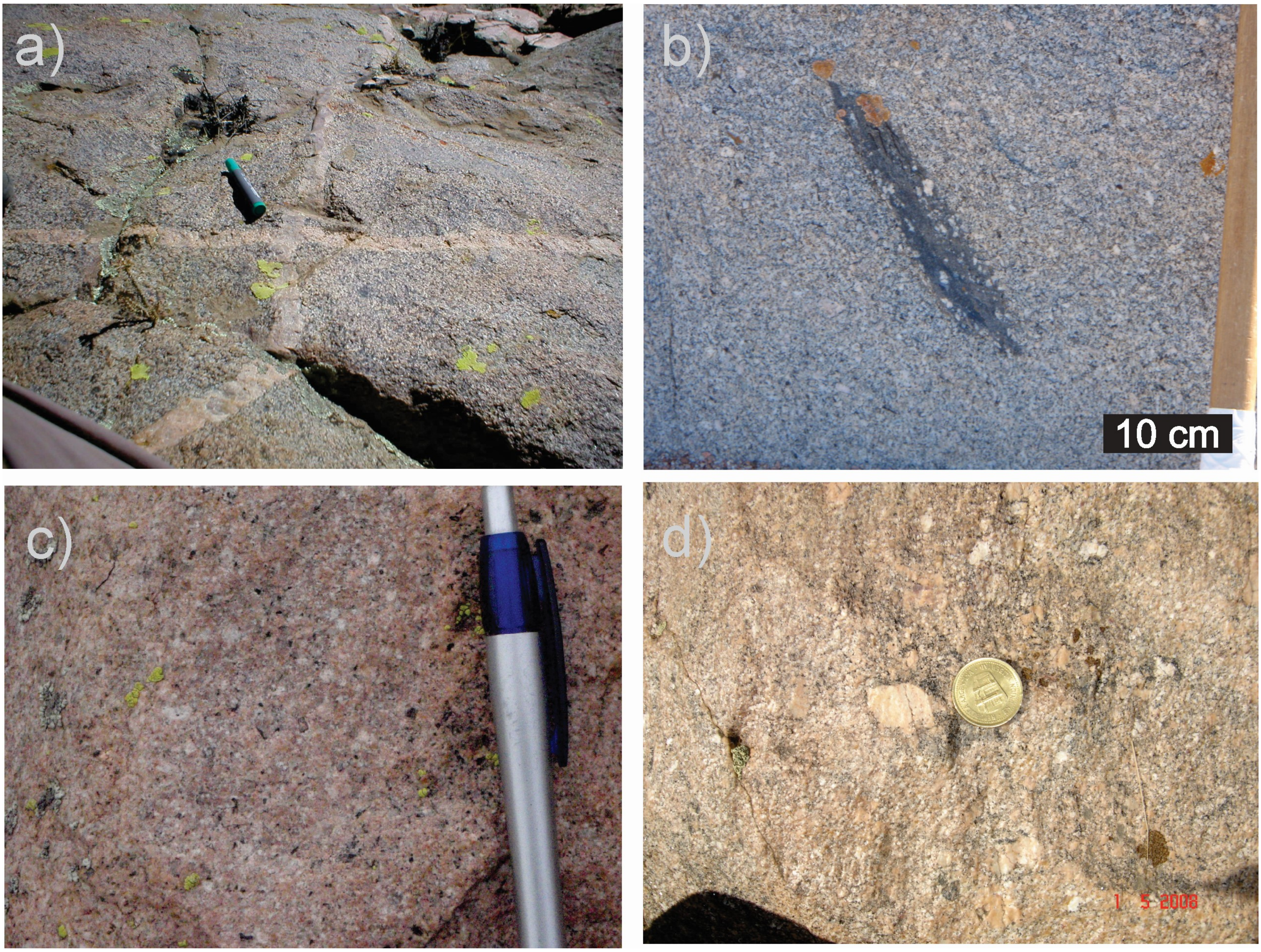
a)
b)
10 cm
c)
d)
1 5 2008


a)
b)
c)
d)

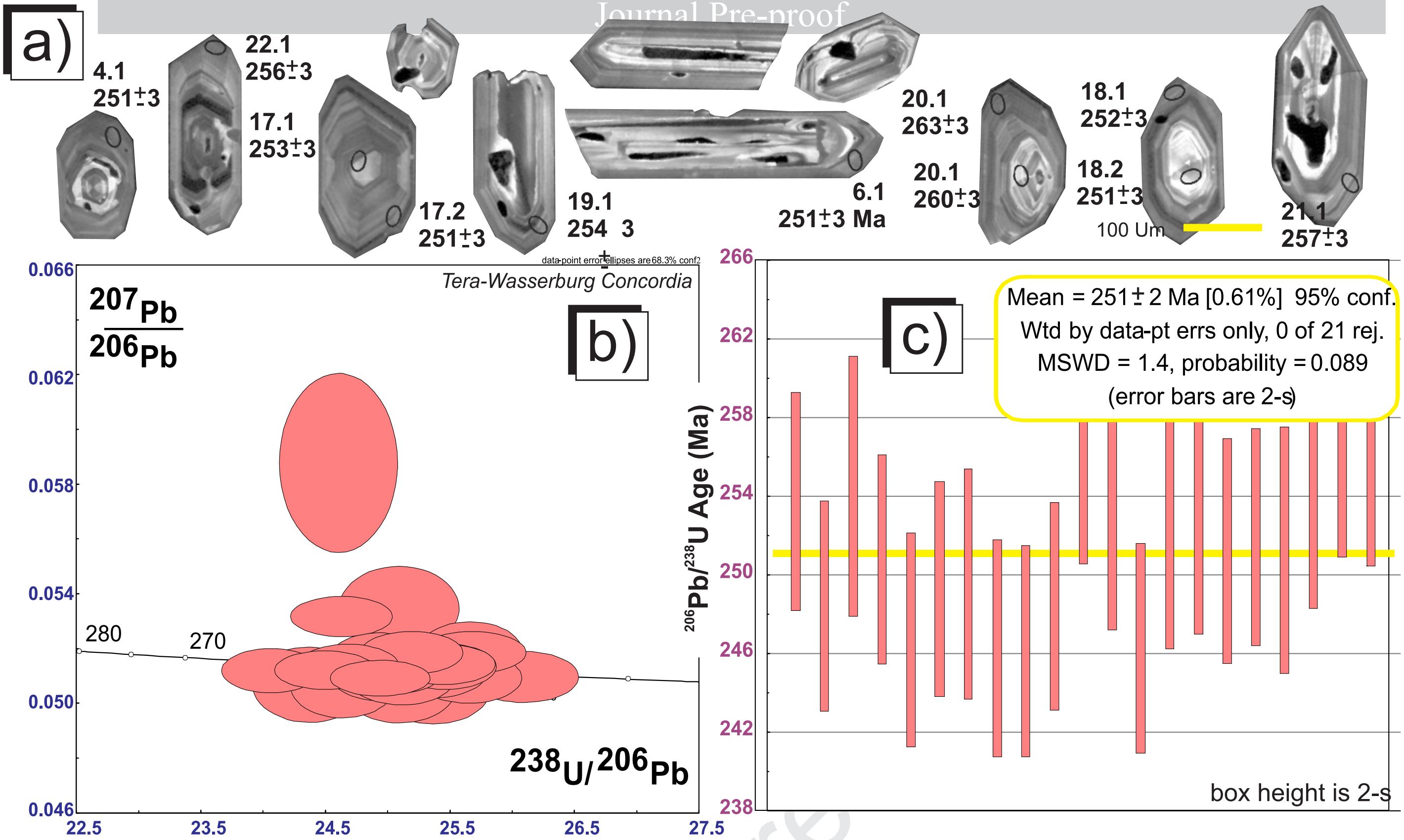
a)
4.1
251±3
22.1
256±3
17.1
253±3
17.2
251±3
19.1
254 3
6.1
251±3 Ma
20.1
263±3
20.1
260±3
18.1
252±3
18.2
251±3
100 Um
21.1
257±3
b)
Tera-Wasserburg Concordia
data-point error ellipses are 68.3% conf.
207Pb/206Pb
238U/206Pb
280
270
0.066
0.062
0.058
0.054
0.050
0.046
22.5
23.5
24.5
25.5
26.5
27.5
c)
Mean = 251±2 Ma [0.61%] 95% conf.
Wtd by data-pt errs only, 0 of 21 rej.
MSWD = 1.4, probability = 0.089
(error bars are 2-s)
206Pb/238U Age (Ma)
266
262
258
254
250
246
242
238
box height is 2-s

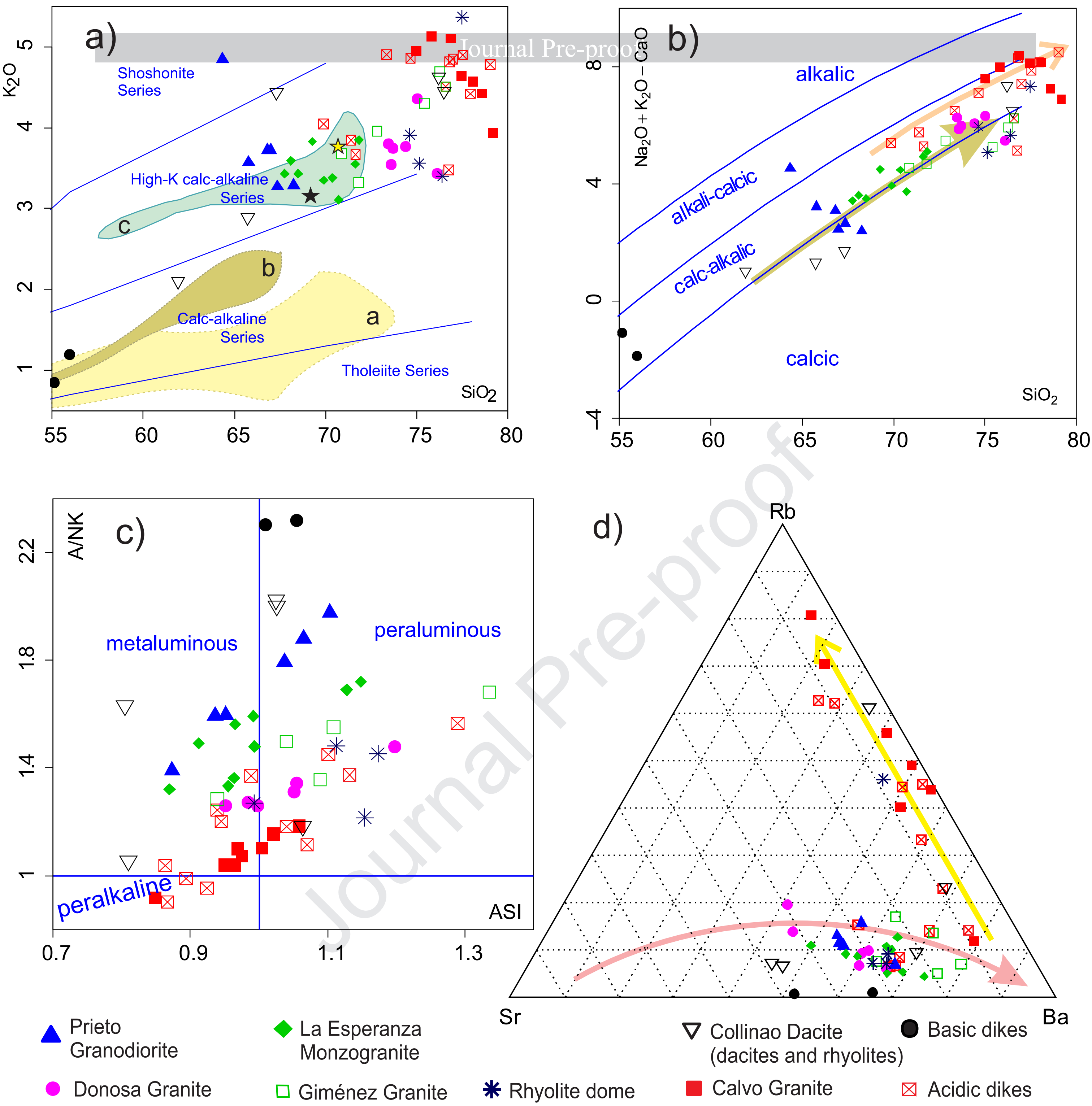

a)
K_2O
Shoshonite Series
High-K calc-alkaline Series
Calc-alkaline Series
Tholeiite Series
SiO_2
b)
$Na_2O + K_2O - CaO$
alkalic
alkali-calcic
calc-alkalic
calcic
SiO_2
c)
A/NK
metaluminous
peraluminous
peralkaline
ASI
d)
Rb
Sr
Ba
Prieto Granodiorite
La Esperanza Monzogranite
Collinao Dacite (dacites and rhyolites)
Basic dikes
Donosa Granite
Giménez Granite
Rhyolite dome
Calvo Granite
Acidic dikes

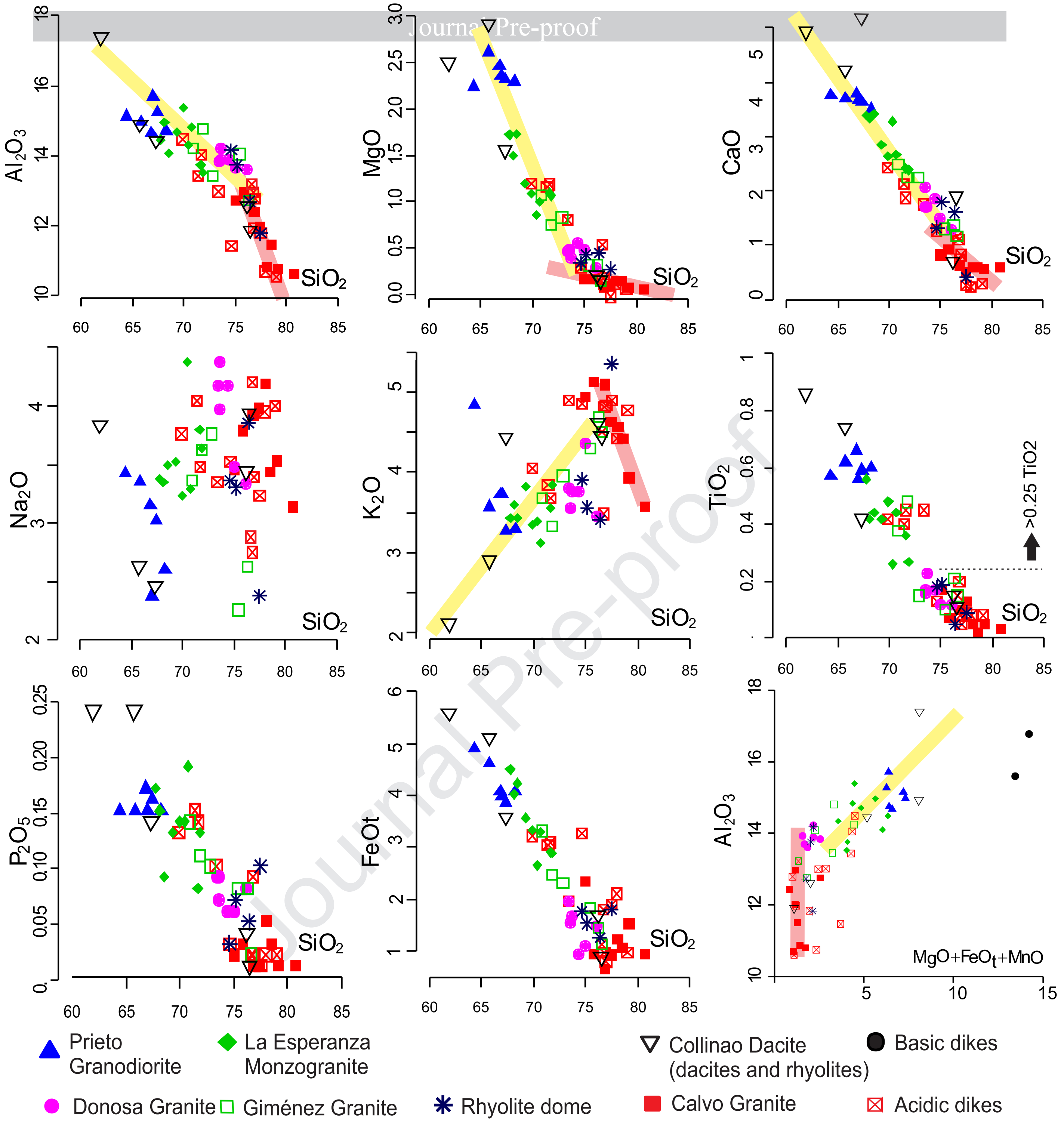

Al2O3
SiO2
MgO
SiO2
CaO
SiO2
Na2O
SiO2
K2O
SiO2
TiO2
SiO2
>0.25 TiO2
P2O5
SiO2
FeOt
SiO2
Al2O3
MgO+FeOt+MnO
Prieto Granodiorite
La Esperanza Monzogranite
Collinao Dacite (dacites and rhyolites)
Basic dikes
Donosa Granite
Giménez Granite
Rhyolite dome
Calvo Granite
Acidic dikes

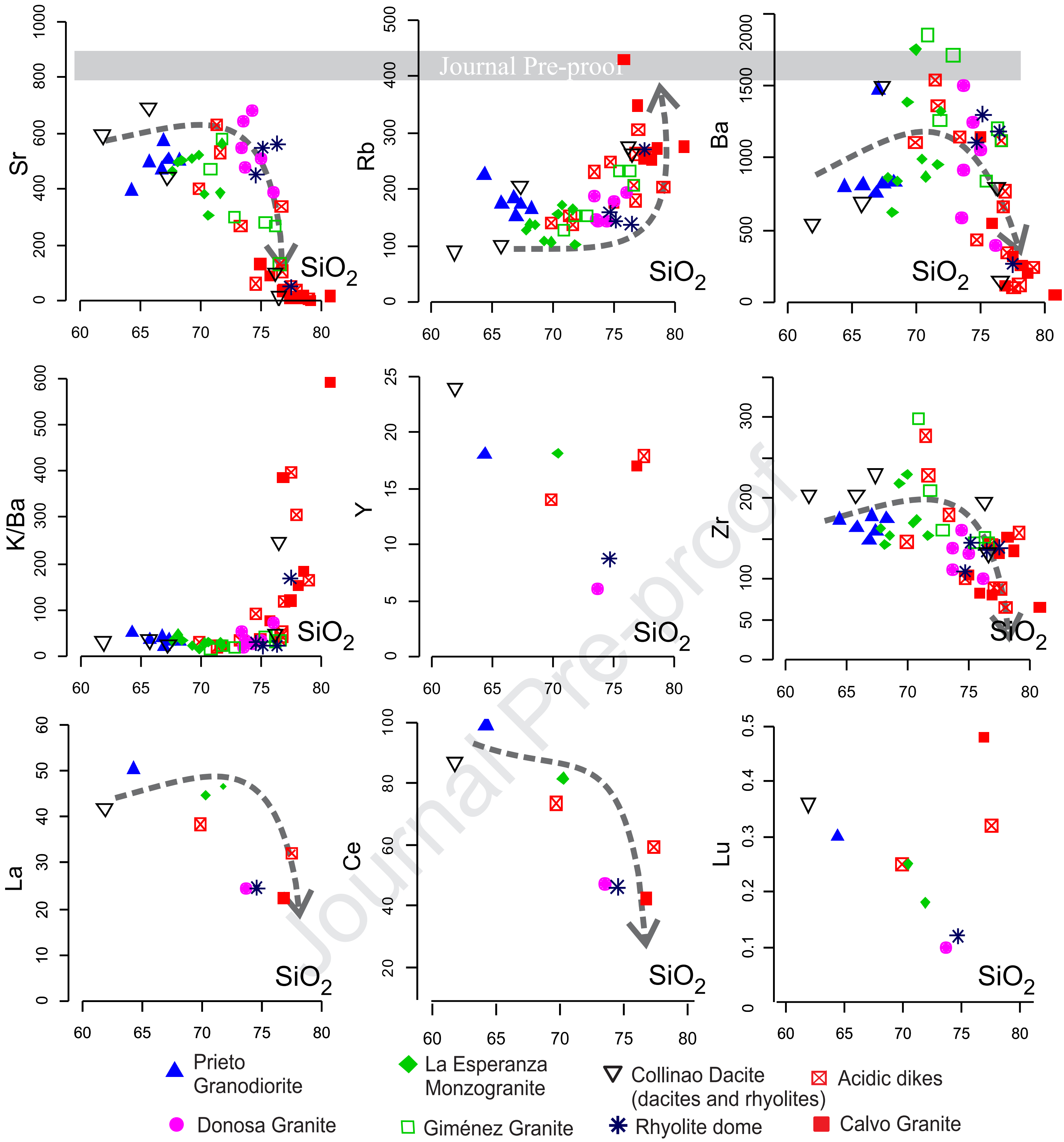
Sr
Rb
Ba
K/Ba
Y
Zr
La
Ce
Lu
SiO2
Prieto Granodiorite
La Esperanza Monzogranite
Collinao Dacite (dacites and rhyolites)
Acidic dikes
Donosa Granite
Giménez Granite
Rhyolite dome
Calvo Granite

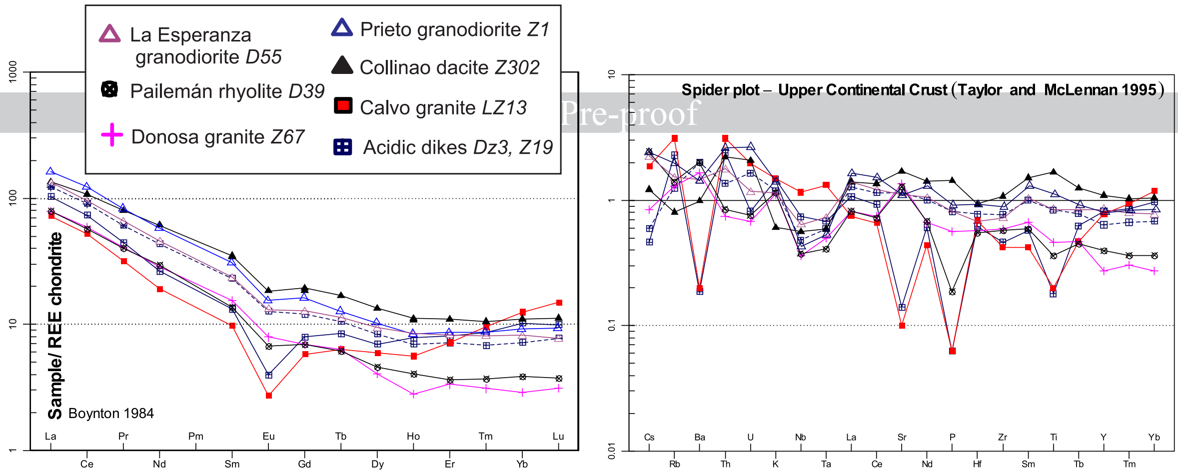
La Esperanza granodiorite D55
Pailemán rhyolite D39
Donosa granite Z67
Prieto granodiorite Z1
Collinao dacite Z302
Calvo granite LZ13
Acidic dikes Dz3, Z19
Sample/ REE chondrite
Boynton 1984
1000
100
10
1
La Ce Pr Nd Pm Sm Eu Gd Tb Dy Ho Er Tm Yb Lu
Spider plot – Upper Continental Crust (Taylor and McLennan 1995)
10
1
0.1
0.01
Cs Rb Ba Th U K Nb Ta La Ce Sr Nd P Hf Zr Sm Ti Tb Y Tm Yb

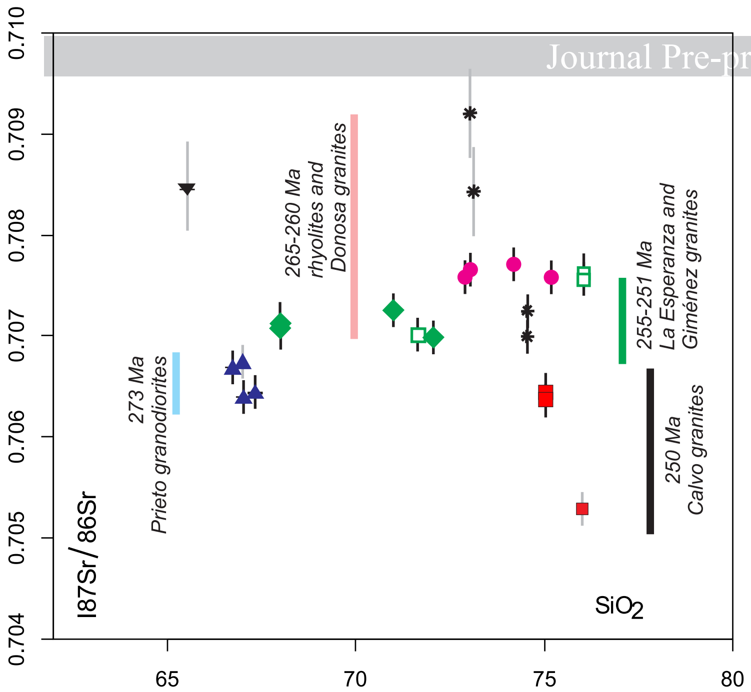
0.710
0.709
0.708
0.707
0.706
0.705
0.704
I87Sr/86Sr
65
70
75
80
SiO2
273 Ma
Prieto granodiorites
265-260 Ma
rhyolites and
Donosa granites
255-251 Ma
La Esperanza and
Giménez granites
250 Ma
Calvo granites

HIGHLIGHTS

- High and low Ba-Sr high-K magnesian calc-alkaline series in La Esperanza plutonic-volcanic complex
- U-Pb zircon dating of Giménez Granite yielded 251 ± 2 Ma
- La Esperanza plutonic-volcanic complex and Los Menucos Group make a up a 273-245 Ma medium-sized silicic large igneous province